Shape Control of Composite Structures with Optimally Placed Piezoelectric Patches

by

Ramesh Periasamy

A thesis

presented to the University of Waterloo

in fulfillment of the

thesis requirement for the degree of

Master of Applied Science

in

Mechanical Engineering

Waterloo, Ontario, Canada, 2008

Author's Declaration for Electronic Submission of a Thesis

I hereby declare that I am the sole author of this thesis. This is a true copy of the thesis, including any required final revisions, as accepted by my examiners. I understand that my thesis may be made electronically available to the public.

Ramesh Periasamy

Abstract

The problem of shape control of composite laminated smart structures with piezoelectric patches placed at optimal location is considered in this thesis. Laminated plate structures with piezoelectric patches for shape control applications are modeled using a shear deformable plate formulation by including the piezoelectric layers into the plate substrate. A composite plate finite element model is also developed for composite plates with self-sensing actuators. Non-linear hysteresis models for piezoelectric materials are presented and discussed. Numerical simulation of composite plate structures with piezoelectric actuators is conducted and presented. The optimization problem of finding the optimal location of actuators using a linear quadratic control algorithm is done and the results are discussed. Static shape control strategies are also discussed.

Contents

List of Figures

List of Tables

Nomenclature

u, v, w	- Displacements in x, y and z directions
σ_{ij},ϵ_{ij}	- Stress and strain components
ϕ_x, ϕ_y	- Rotation of mid-plane about x and y axes
$[Q]$	- Material coefficients
$q(x, y)$	- Uniformly distributed load
$\{N\}$	- In-plane force resultant
$\{M\}$	- Moment resultant
$\{T\}$	- Transverse force resultant
s	- Shear correction factor
$[A_{ij}], [B_{ij}], [D_{ij}]$	- Extensional, bending and coupling stiffnesses
$\{u\}^e$	- Element displacement vector
H_i	- Shape functions
$[M]$	- Mass matrix

$[K]$ - Stiffness matrix

$[\mathcal{C}]$ - Damping matrix

$\{F\}$ - Force vector

η, δ - Damping coefficients

Y_{ij}, G_{ij} - Young's modulus and shear modulus

ν - Poisson's ratio

$[\bar{e}]$ - Piezoelectric stress coefficients

$[\mathcal{D}]$ - Electric displacement

$\{E_i\}$ - Electric field vector

$\{V\}$ - Electric potential

q - Total electric charge

P - Polarization

$\mathsf{A}, \mathsf{B}, \mathsf{D}$ - System matrices

W - Controllability grammian

S - Solution of algebraic Riccati equation

$[\mathsf{Q}], [\mathsf{R}]$ - Weighting matrices

Chapter 1

Introduction

In recent years development of self-sensing and self-correcting high-performance structures has been motivated by the various needs of modern aeronautical, automobile and space industries. A structure with embedded actuation unit, sensor unit and a control system that changes its shape and dynamic behavior in response to any change in the external environment can be termed as smart or intelligent structure. Such structures use special materials called smart materials as actuating and sensing elements. Materials with special properties such as changing shape when heated or electrified, producing electricity when compressed or heated, and changing their physical states when subject to a magnetic or electric field are called smart materials. Some of these properties can be manipulated and used effectively in the actuation and sensing. Bonding or embedding these smart materials into structures gives the inherent self-sensing and self-correcting ability without any separate sensing or actuation unit.

One of the materials that can be used as an actuator and sensor is piezoelectric material. Piezoelectric materials generate an electric charge when subjected to mechanical deformation (direct piezoelectricity), and conversely produce mechanical strain under an applied

electric field (converse piezoelectricity). The use of piezoelectric materials as actuators and sensors has been successfully demonstrated by many researchers during the last decade. The coupled electromechanical properties of the piezoelectric materials, high strain rates, simple mechanism of actuation, and their availability in different shapes and in synthetic forms has made it possible to use them as one of the important actuation and sensing elements in structural control applications. Magnetostrictive material, shape-memory alloys, and magnetoreheological fluids are some of the other smart materials in use today.

In addition, modern space, automotive and aircraft structures need to be strong but light weight. Composites, in which two or more different materials with different material properties and/or chemical properties are put together in some particular fashion and tailored to meet the required engineering properties, are promising for such applications. Due to their high stiffness to weight ratio, strength to weight ratio and ability to withstand high temperatures, composite materials are very attractive for modern structural needs. By embedding piezoelectric elements into composite material structures, there are possibilities of creating high-performance flexible structures with high strength, high stiffness and light weight with self-sensing and self-correcting ability. Two different ways of embedding piezoelectric elements into the structures have been employed in the past for the structural control, (1) placing the piezoelectric elements over the entire structure, and (2) placing them at selected locations. The selective placement method has been proven to be more economical and effective [38].

Smart structures are used in several shape and vibration control applications. Micropositioning, satellite antenna shape control, space structure shape correction, and automatic flow control valves are some of the practical examples of shape control applications. Active vibration suppression in aircraft and active suspension systems for vehicles are some of the vibration control applications. There are several concerns in these applications: (1)

What material should be used in base structure? (2) What type of actuators should be used? (3) Where to place the actuators and how many? (4) How to control the system and what is the accuracy? (5) How to model and analyze, What is the required model accuracy? and (6) Issues related to the experimental verification of the model. All of these remain as open questions and many researchers are involved in finding answers to these questions.

Advanced computer modelling techniques allow us to simulate the aforementioned smart structures, compute the optimal placement of the actuating elements, and examine the system performance. A sophisticated and accurate structural model is needed for the optimization algorithms and control system simulations. Finite element techniques are used extensively to model and analyze such structures.

The goal of the thesis is to study the shape control of composite smart structures with optimally placed self-sensing piezoelectric patches. Shape control is a process of driving the system to a desired or initial shape with piezoelectric actuators and sensors from the current or the disturbed shape. In order to achieve the goal, the following studies will be conducted: (1) Development of a comprehensive finite element model for composite plate structures embedded with self-sensing piezoelectric patches considering geometrical non-linearities and electro-mechanical hysteresis, (2) Optimization to find optimal locations of piezoelectric patches. This thesis presents the background information and work done to achieve the proposed goals on finite element modelling, and control and optimization with their numerical simulations.

Finite element modelling:

A finite element model is developed to study the layered composite plates with piezoelectric patches. Geometric non-linearities and shear deformations are considered to achieve higher accuracy and to account for moderately thick plate substrates. One of the problems in

shape control and micro-positioning is the loss of accuracy due to the electromechanical hysteresis of piezoelectric materials. Self-sensing actuator concept, in which a single piece of piezoelectric element is used as actuator and sensor, is also incorporated in the developed finite element. Comparison results to validate the finite element and numerical simulations of composite plate structures with linear piezoelectric actuator models are conducted and presented.

Control and optimization

A linear quadratic regulator based optimization algorithm is used for finding the optimal location of one actuator on a beam. Dynamic behavior of the beam with the actuator placed at the optimal location is presented. Numerical simulations for optimal locations of the actuator are presented for the static shape control applications.

In Chapter 2, basic theories used in the modelling of composite plates are discussed. Special mention is given to thick plate modelling with shear deformation theory. A finite element model developed to model composite plates is given at the end of the chapter. Some of the fundamentals about piezoelectric materials and their use as actuator, and a finite element model for composite plates with linear piezoelectric patches based on the element developed in the previous chapter is given in Chapter 3. Hysteresis models and self-sensing techniques are discussed at the end of Chapter 3. Different control objectives used in constructing the cost function for optimizing patch locations are given in Chapter 4 with a few optimization algorithms for static and dynamic shape control application. Summary and discussions are given in the last chapter.

Chapter 2

Plate Theory and Finite Element Modelling

Modern automotive, aerospace and space industries require new materials with unique characteristics such as high weight to strength ratio, high tensile strength in some specific directions etc. Plate structures with much smaller dimension in one direction than the other two, are one of the main structural elements in these applications. Layered composite plate structures have the special properties required in these applications and hence are used most widely. Composite plate structures are modeled using plate theories. Classical plate theories give good results for thin plates. When the aspect ratio of the plate increases, the transverse shear effects should be considered in the model for better results. Since the composite plates are used as the base structure in this work, this chapter reviews the basic theories for plate structures with more focus on the higher order theories for modelling thick layered composite plates.

The finite element method (FEM), used to solve the differential equations governing structural behavior, is also reviewed in this context. Its development and numerical solution

of layered composite plate structures are explained along with the element formulation. Linear and nonlinear results are given with validation and comparison.

2.1 First order shear deformation plate theory

Plate structures which are three dimensional structural members frequently encountered in engineering applications. Due to the smaller dimension in the thickness direction when compared to the other dimensions, plate problems can be solved using plane stress assumptions. In the plane stress assumptions: (1) the displacement variation in thickness direction is assumed to be zero, (2) the stresses in the thickness direction are negligible (very small magnitude). Figure 2.1 explains the plane state of stress on a cross-section of a thin slab.

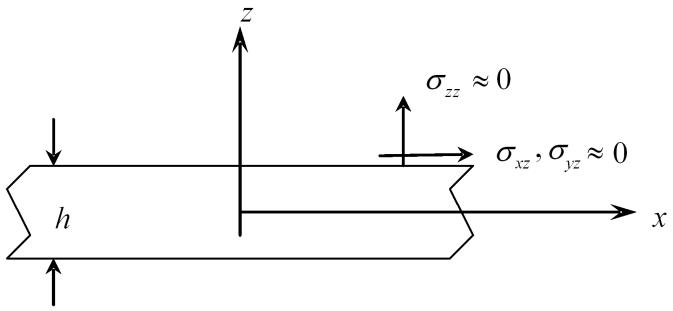

Figure 2.1: Plane state of stress

The basic theory for plate problems, *classical plate theory* or *Kirchhoff's theory* is based on the *Kirchhoff's hypothesis*: (1) straight lines perpendicular to the mid-surface (i.e. transverse normals) remain straight before and after deformation and their in-extensibility, (2) transverse normals rotate to remain perpendicular to the mid-surface. Thus the deformation is assumed to be entirely due to bending and in-plane stretching. The effect of

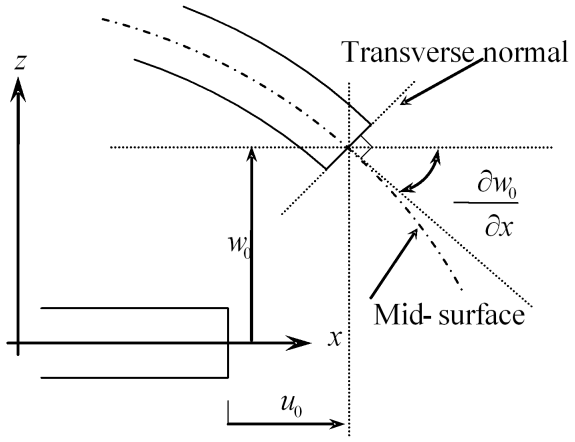

Figure 2.2: Deformed and un-deformed shape with classical plate theory

transverse shear and transverse normals are neglected. Figure 2.2 displays the classical plate theory; it shows that the transverse normals remain perpendicular to the mid-surface before and after deformation.

When the thickness of the plate increases, the transverse shear strains should be included in the theory. The first-order shear deformation theory accounts for the transverse shear strain by assuming that it is constant with respect to the thickness coordinate [50]. It is not assumed that the transverse normals remain perpendicular to the mid-surface after deformation. First order shear deformation theory gives better results for thick plates (plates with higher aspect ratio) while the classical plate theory is sufficient to predict deformations for thin plates. Third and higher order theories were also proposed by relaxing all the constraints imposed by *Kirchhoff's hypothesis.* However, for very large thicknesses three-dimensional elasticity yields better results than these higher-order plate theories [50]. In this thesis layered composite plates with moderate thickness with geometric non-linearity are used, and so the nonlinear first-order shear deformation theory [50] is explained here.

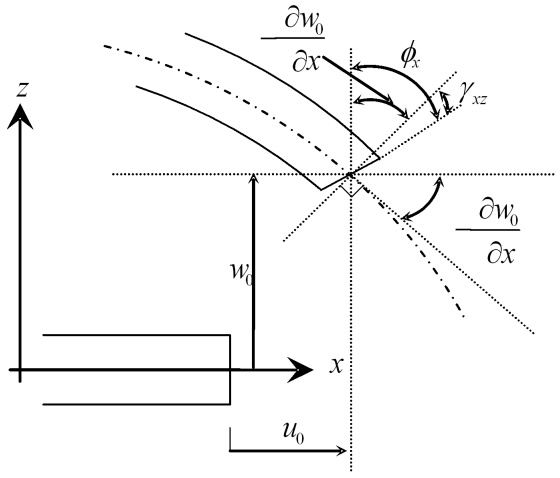

Figure 2.3: Deformed and un-deformed shape with first order theory

The deformed and un-deformed shape of a plate and the notations used are explained in Figure 2.3, based on the first order shear deformation theory assumptions . The displacements (u, v, w) in the x, y and z directions respectively are expressed as functions of mid-plane translations (u_0, v_0, w_0) and independent normal rotations (ϕ_x, ϕ_y) as:

$$\begin{aligned} u(x, y, z, t) &= u_0(x, y) + z\phi_x(x, y, t) \\ v(x, y, z, t) &= v_0(x, y) + z\phi_y(x, y, t) \\ w(x, y, z, t) &= w_0(x, y) \end{aligned} \tag{2.1}$$

where, ϕ_x, and ϕ_y are the rotations of the normal with respect to the un-deformed mid-plane in the xz and yz planes, respectively. These normals are not necessarily perpendicular to the mid-plane after deformation, according to the first order theory assumptions, and consequently shear deformation is permitted. The nonlinear strains associated with the

displacement field can be written from the general Green strain expression for the three dimensional state of stress. With the assumptions of small strains (the squares and products of strains are negligible) and moderate rotations, the geometric nonlinear strains (von Karman) can be written as:

$$\begin{aligned}
\epsilon_{xx} &= \frac{\partial u_0}{\partial x} + \frac{1}{2}\left(\frac{\partial w_0}{\partial x}\right)^2 - z\frac{\partial \phi_x}{\partial x} \\
\epsilon_{yy} &= \frac{\partial v_0}{\partial y} + \frac{1}{2}\left(\frac{\partial w_0}{\partial y}\right)^2 - z\frac{\partial \phi_y}{\partial y} \\
\epsilon_{xy} &= \left(\frac{\partial u_0}{\partial y} + \frac{\partial v_0}{\partial x}\right) + \left(\frac{\partial w_0}{\partial x}\frac{\partial w_0}{\partial y}\right) - z\left(\frac{\partial \phi_x}{\partial y} + \frac{\partial \phi_y}{\partial x}\right) \\
\epsilon_{yz} &= \frac{\partial w_0}{\partial y} + \phi_x \\
\epsilon_{xz} &= \frac{\partial w_0}{\partial x} + \phi_y.
\end{aligned} \tag{2.2}$$

By collecting the in-plane strains, linear (ϵ_p) and nonlinear (ϵ_p^{nl}), bending strain (ϵ_b), and shear strain (ϵ_s) terms, the total strain can be written in a compact form as follows:

$$\begin{aligned}
\{\epsilon\} &= \left\{ \begin{Bmatrix} \epsilon_p \\ 0 \end{Bmatrix} + \begin{Bmatrix} -z\epsilon_b \\ \epsilon_s \end{Bmatrix} \right\} + \begin{Bmatrix} \epsilon_p^{nl} \\ 0 \end{Bmatrix} \\
&= \left\{ \{\epsilon^l\} + \{\epsilon^{nl}\} \right\}
\end{aligned} \tag{2.3}$$

where,

$$\epsilon_p = \begin{Bmatrix} \frac{\partial u_0}{\partial x} \\ \frac{\partial v_0}{\partial y} \\ \frac{\partial u_0}{\partial y} + \frac{\partial v_0}{\partial x} \end{Bmatrix} \qquad \epsilon_b = \begin{Bmatrix} \frac{\partial \phi_x}{\partial x} \\ \frac{\partial \phi_y}{\partial y} \\ \frac{\partial \phi_x}{\partial y} + \frac{\partial \phi_y}{\partial x} \end{Bmatrix}$$

$$\epsilon_s = \begin{Bmatrix} \frac{\partial w_0}{\partial y} + \phi_x \\ \frac{\partial w_0}{\partial x} + \phi_y \end{Bmatrix} \qquad \epsilon_p^{nl} = \begin{Bmatrix} \frac{1}{2}\left(\frac{\partial w_0}{\partial x}\right)^2 \\ \frac{1}{2}\left(\frac{\partial w_0}{\partial y}\right)^2 \\ \left(\frac{\partial w_0}{\partial x}\frac{\partial w_0}{\partial y}\right) \end{Bmatrix}$$

here the superscripts l denotes the linear strain and nl denotes the nonlinear strains.

2.2 Layered Composite Plates

Composite materials are made by combining two or more materials to achieve the desired properties such as stiffness, strength, weight reduction, thermal properties for the structure. Usually the reinforcing material is called *fiber* and the medium or the base material is called *matrix* which may be metallic or nonmetallic. The stiffness and strength of the composite materials come from the fiber which are usually stronger than the matrix materials. A composite material layer called *lamina* (or ply) is a sheet of composite material, which is usually made of two or more constituents and considered generally as orthotropic.

Layered composite plates are made by stacking a number of composite laminas in a desired sequence, called a lamination scheme. Usually the lamination scheme is represented with the ply angles of all the layers, for example a three layer orthotropic composite plate may be represented as $(0°/90°/0°)$. A unidirectional fiber-reinforced lamina is formed by embedding the continuous fiber materials in the matrix materials in one particular direction. They exhibit high strength in the direction of the fiber and are weak in the direction perpendicular to the fiber. Composite plates are custom made to the requirements by stacking many layers in different sequence to adjust the resulting properties. With the assumptions of lamina as a continuum and an elastic material, the generalized Hooke's law for a composite lamina can be written as

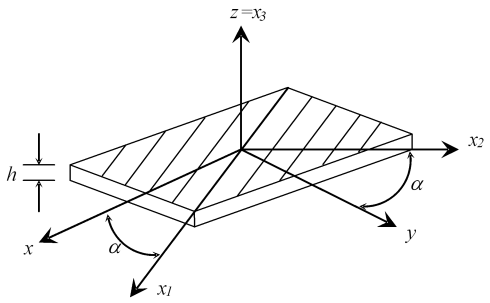

Figure 2.4: Lamina with materials and problem coordinates

$$\{\sigma_{ij}\} = [Q]\{\epsilon_{ij}\} \tag{2.4}$$

where $\{\sigma_{ij}\}$ are the stress components and $\{\epsilon_{ij}\}$ are the strain components and $[Q]$ are material coefficients. The uni-directional fiber-reinforced composite lamina is considered as an orthotropic material with its material coordinate axis x_1 be taken parallel to the fiber direction and axis x_2 to be perpendicular to the fiber direction and the axis x_3 is perpendicular to the plane of the lamina. Often, the material coordinates (x_1, x_2, x_3) and the problem coordinates (x, y, z) will not be the same. Also, composite plates may have many different layers with different stacking sequence. Figure 2.4 shows such a lamina. The material coefficients should then be transformed to the problem coordinates using the ply angle α for each lamina. The transformation details are in Appendix A. The constitutive equation of an orthotropic layer transformed to the problem coordinate is given as:

$$\{\sigma_{ij}\} = \left[\overline{Q}_{ij}\right]\{\epsilon_{ij}\} \tag{2.5}$$

where $\overline{Q}_{ij}$ are transformed material coefficients of the layer in the problem coordinates as given in Appendix A, σ_{ij} and ϵ_{ij} are stresses and strains respectively for the lamina.

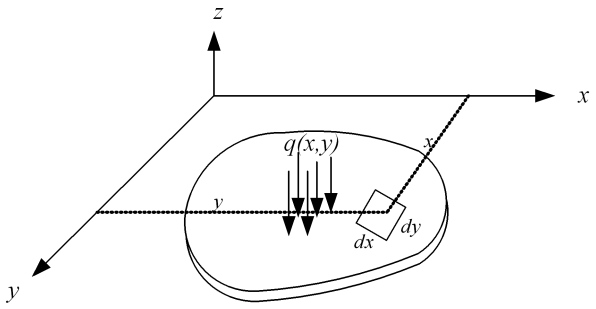

Figure 2.5: Plate with distributed load

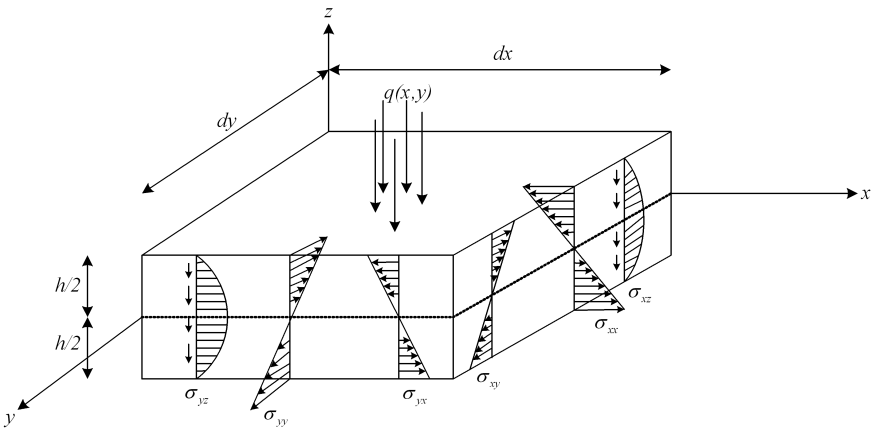

Figure 2.6: Stress distribution in the plate element

The three dimensional plate is usually idealized to the mid-surface and the bending of that mid-surface is studied. Consider an element ($dx \times dy \times h$) of the loaded plate (distributed load, $q(x, y)$) with thickness h for the idealization. The stress distributions across the thickness in such an element is shown in Figure 2.6. The positive force and moment resultants per unit length transferred to the mid-plane of the element due to the distribution of stresses across the thickness are shown in the Figure 2.7. The governing equations of motion based on first order shear deformation theory can be derived from the principle of virtual work, which may be stated as:

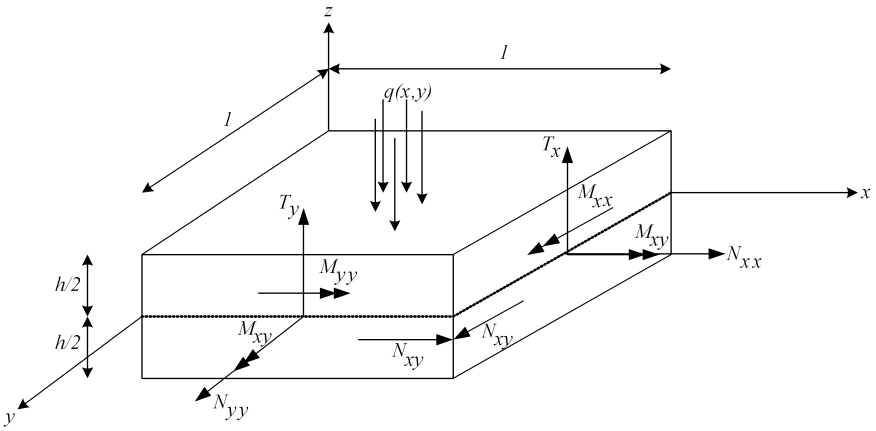

Figure 2.7: Positive resultants and load on a plate element

$$0 = \int_0^T (\delta U + \delta V - \delta K) dt \tag{2.6}$$

where δU is the virtual strain energy, δV is the virtual work done by the applied forces and δK is the virtual kinetic energy. By substituting the expressions for virtual energies in terms of stresses and strains we obtain the equations of motion. The in-plane force resultants $\{N\}$, moment resultants $\{M\}$, the transverse force resultants $\{T\}$ and the mass moment of inertias (I_0, I_1, I_2) can be written as:

$$\{N\} = \begin{Bmatrix} N_{xx} \\ N_{yy} \\ N_{xy} \end{Bmatrix} = \int_{-h/2}^{h/2} \begin{Bmatrix} \sigma_{xx} \\ \sigma_{yy} \\ \sigma_{xy} \end{Bmatrix} dz \qquad \{M\} = \begin{Bmatrix} M_{xx} \\ M_{yy} \\ M_{xy} \end{Bmatrix} = \int_{-h/2}^{h/2} \begin{Bmatrix} \sigma_{xx} \\ \sigma_{yy} \\ \sigma_{xy} \end{Bmatrix} z dz$$

$$\{T\} = \begin{Bmatrix} T_x \\ T_y \end{Bmatrix} = \mathrm{s} \int_{-h/2}^{h/2} \begin{Bmatrix} \sigma_{xz} \\ \sigma_{yz} \end{Bmatrix} dz \qquad \begin{Bmatrix} I_0 \\ I_1 \\ I_2 \end{Bmatrix} = \int_{-h/2}^{h/2} \begin{Bmatrix} 1 \\ z \\ z^2 \end{Bmatrix} \rho dz \tag{2.7}$$

where s is the shear correction factor which usually takes the value of 5/6 [50] and ρ is

the density of the material. The Euler-Lagrange equations are obtained by setting the coefficients of the virtual displacements in the virtual work to zero independently:

$$\begin{aligned}
\delta u_0: &\quad \frac{\partial N_{xx}}{\partial x}+\frac{\partial N_{xy}}{\partial y}=I_0\frac{\partial^2 u_0}{\partial t^2}+I_1\frac{\partial^2 \phi_x}{\partial t^2},\\
\delta v_0: &\quad \frac{\partial N_{yy}}{\partial y}+\frac{\partial N_{xy}}{\partial x}=I_0\frac{\partial^2 v_0}{\partial t^2}+I_1\frac{\partial^2 \phi_y}{\partial t^2},\\
\delta w_0: &\quad \frac{\partial T_x}{\partial x}+\frac{\partial T_y}{\partial y}+\mathcal{N}(w_0)+q(x,y)=I_0\frac{\partial^2 w_0}{\partial t^2},\\
\delta \phi_x: &\quad \frac{\partial M_{xx}}{\partial x}+\frac{\partial M_{xy}}{\partial y}-T_x=I_2\frac{\partial^2 \phi_x}{\partial t^2}+I_1\frac{\partial^2 u_0}{\partial t^2},\\
\delta \phi_y: &\quad \frac{\partial M_{yy}}{\partial y}+\frac{\partial M_{xy}}{\partial x}-T_y=I_2\frac{\partial^2 \phi_y}{\partial t^2}+I_1\frac{\partial^2 v_0}{\partial t^2}.
\end{aligned} \tag{2.8}$$

In the equations $q(x,y)$ is the distributed load applied to the plate and the term $\mathcal{N}(w_0)$ can be written as:

$$\mathcal{N}(w_0)=\frac{\partial}{\partial x}\left(N_{xx}\frac{\partial w_0}{\partial x}+N_{xy}\frac{\partial w_0}{\partial y}\right)+\frac{\partial}{\partial y}\left(N_{yy}\frac{\partial w_0}{\partial y}+N_{xy}\frac{\partial w_0}{\partial x}\right).$$

For a general composite laminated plate, consisting of n layers having different material properties, stresses vary through the thickness because of the change in material coefficients. Therefore the integration through the thickness should be done layer by layer. The in-plane force resultants $\{N\}$, moment resultants $\{M\}$ and the transverse force resultants $\{T\}$ for a general laminated composite plate become:

$$\{N\}=\begin{Bmatrix} N_{xx}\\ N_{yy}\\ N_{xy}\end{Bmatrix}=\sum_{k=1}^{n}\int_{z_k}^{z_{k+1}}\begin{Bmatrix}\sigma_{xx}\\ \sigma_{yy}\\ \sigma_{xy}\end{Bmatrix}dz$$

$$\{M\} = \left\{ \begin{array}{c} M_{xx} \\ M_{yy} \\ M_{xy} \end{array} \right\} = \sum_{k=1}^{n} \int_{z_k}^{z_{k+1}} \left\{ \begin{array}{c} \sigma_{xx} \\ \sigma_{yy} \\ \sigma_{xy} \end{array} \right\} z dz$$

$$\{T\} = \left\{ \begin{array}{c} T_x \\ T_y \end{array} \right\} = \mathrm{s} \sum_{k=1}^{n} \int_{z_k}^{z_{k+1}} \left\{ \begin{array}{c} \sigma_{xz} \\ \sigma_{yz} \end{array} \right\} dz. \tag{2.9}$$

By substituting the constitutive equation (2.5) into equation (2.9) and using equations (2.2) and (2.3), the resultants can be written as follows:

$$\left\{ \begin{array}{c} \{N\} \\ \{M\} \\ \{T\} \end{array} \right\} = \left[\begin{array}{ccc} [A_{ij}] & [B_{ij}] & 0 \\ [B_{ij}] & [D_{ij}] & 0 \\ 0 & 0 & \mathrm{s}[S] \end{array} \right] \left\{ \begin{array}{c} \epsilon_p \\ \epsilon_b \\ \epsilon_s \end{array} \right\} \tag{2.10}$$

where $[A_{ij}]$, $[B_{ij}]$ and $[D_{ij}]$ matrices are defined as:

$$[A_{ij}] = \sum_{k=1}^{n} \int_{z_k}^{z_{k+1}} \bar{Q}_{ij}^{k} z dz \tag{2.11}$$

$$[B_{ij}] = \sum_{k=1}^{n} \int_{z_k}^{z_{k+1}} \bar{Q}_{ij}^{k} z dz \tag{2.12}$$

$$[D_{ij}] = \sum_{k=1}^{n} \int_{z_k}^{z_{k+1}} \bar{Q}_{ij}^{k} z^2 dz \tag{2.13}$$

and,

$$[S] = \left[\begin{array}{cc} A_{44} & A_{45} \\ A_{45} & A_{55} \end{array} \right] \tag{2.14}$$

where the extensional stiffness are defined as:

$$\begin{aligned} A_{44} &= \sum_{k=1}^{n} \int_{z_k}^{z_{k+1}} \bar{Q}_{44}^{k} dz \\ A_{45} &= \sum_{k=1}^{n} \int_{z_k}^{z_{k+1}} \bar{Q}_{45}^{k} dz \\ A_{55} &= \sum_{k=1}^{n} \int_{z_k}^{z_{k+1}} \bar{Q}_{55}^{k} dz \end{aligned}$$

where $\bar{Q}_{ij}^{k}$ are transformed material coefficients of layer k. By substituting the resultant equations into the equation of motion (2.8) they can be written in terms of the displacements.

2.3 Finite element modeling

A typical element with four nodes on the corner in actual (x, y, z) and natural coordinate systems (r, s, t) are shown in Figure 2.8 . Each node is assumed to have five degrees of freedom. Thus, the nodal displacement vector $\{u\}^e$ of an element is represented as:

$$\{u\}^e = \left[\begin{array}{ccccc} u_i & v_i & w_i & \phi_{xi} & \phi_{yi} \end{array} \right]_{i=1...4} \tag{2.15}$$

where u_i, v_i and w_i are the translational degrees of freedom in x, y and z directions of node i respectively. The components ϕ_{xi} and ϕ_{yi} are the rotational degrees of freedom about x and y axes of the same node. Isoparametric formulation is used in the element modeling; that is the geometry and the variation of nodal displacements within the element are written using the same shape functions. The location of any point inside the element (x, y) may be represented in terms of the nodal coordinates (x_i, y_i) of that element using

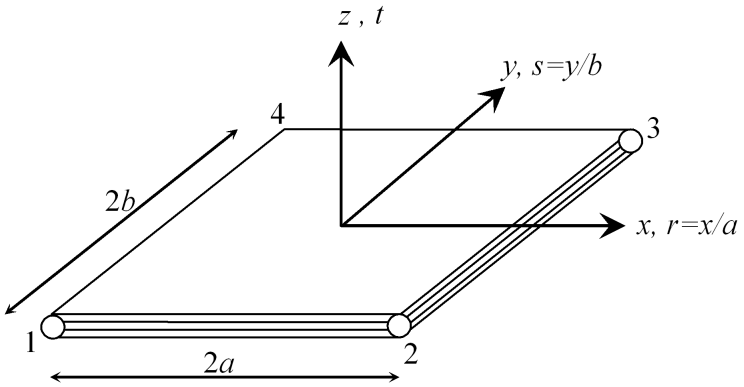

Figure 2.8: Finite element description

the shape functions. Shape functions H_i should take the value 1 at the node i and 0 at the other nodes. They should be continuous inside the element and across the boundaries. The Lagrange shape functions used here take the form,

$$H_i = \frac{1}{4}(1 + rr_i)(1 + ss_i) \tag{2.16}$$

for node i, where r_i and s_i are natural coordinates. The coordinate of any point inside an element in terms of nodal coordinates can be written as:

$$x = \sum_{i=1}^{4} H_i x_i \qquad y = \sum_{i=1}^{4} H_i y_i. \tag{2.17}$$

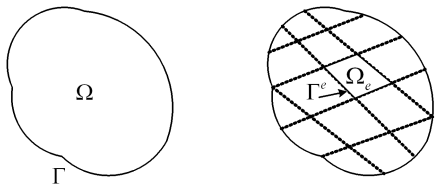

Figure 2.9: Finite Element discretization

The displacements inside the elements also may be represented in terms of their nodal values using the same shape functions used to represent the geometry as:

$$u = \sum_{i=1}^{4} H_i u_i, \qquad v = \sum_{i=1}^{4} H_i v_i, \qquad w = \sum_{i=1}^{4} H_i w_i,$$
$$\phi_x = \sum_{i=1}^{4} H_i \phi_{xi}, \quad \phi_y = \sum_{i=1}^{4} H_i \phi_{yi}.$$

Strain displacement relations were derived from the stress-strain relations (equation (2.2)) using the shape functions. Details are in Appendix B. Equations of motion of an element can be derived from the virtual work principle applied to an elemental area Ω^e as in Figure 2.9.

The virtual work statement (equation (2.6)) can be written as follows after discretization,

$$0 = \sum_{1}^{n_e} \int_0^T (\delta U^e + \delta V^e - \delta K^e) dt \tag{2.18}$$

where n_e is the total number of elements in the discretization. The potential energy, the external work done and the kinetic energy due to virtual displacements on the elemental volume are shown by δU^e, δV^e and δK^e respectively . They can be written as:

$$\delta U^e = \int_V \sigma_{ij} \delta \epsilon_{ij} dV \tag{2.19}$$

$$\delta V^e = -\left(\int_V q\delta u dV + \int_{\Gamma^e} t\delta u ds\right) \tag{2.20}$$

$$\delta K^e = \int_V \rho \frac{\partial^2 u}{\partial t^2}\delta u dV \tag{2.21}$$

where V is elemental volume, Γ^e is the length of the boundary at which the traction t is applied, q is the nodal forces and δu is the virtual displacement. The dynamic equation for an element can be obtained by substituting the strain displacement relations into the virtual work statement,

$$[M]^e \{\ddot{u}\}^e + [K]^e \{u\}^e = \{F\}^e \tag{2.22}$$

where $[M]^e, [K]^e$ and $\{F\}^e$ are mass matrix, stiffness matrix and force vector for an element. Global dynamic equation after assembly becomes:

$$[M] \{\ddot{u}\} + [K] \{u\} = \{F\} \tag{2.23}$$

where $[M], [K]$ and $\{F\}$ are global mass matrix, stiffness matrix and force vector respectively. Structural damping is introduced in the model using Rayleigh damping, i.e. the damping matrix is proportional to the mass and stiffness matrices. The dynamic equation is then

$$[M] \{\ddot{u}\} + [\mathcal{C}] \{\dot{u}\} + [K] \{u\} = \{F\}, \tag{2.24}$$

where

$$[\mathcal{C}] = \eta [M] + \delta [K] \tag{2.25}$$

with damping coefficients η and δ. The matrices and external load vector formulations are given in Appendix B.

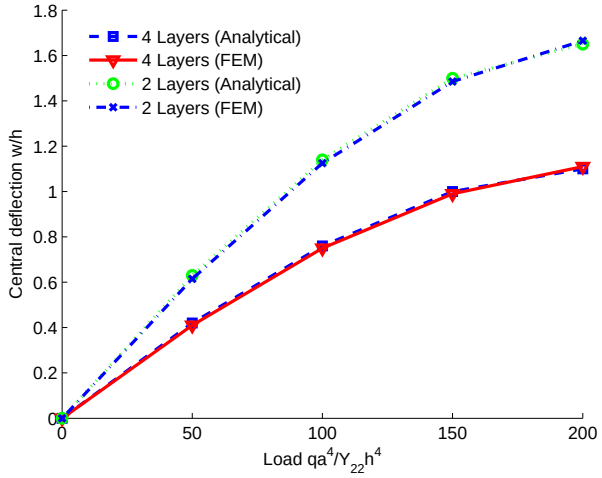

Figure 2.10: Validation of finite element

2.4 Verification

A *Matlab* code was written based on the finite element model presented earlier for numerical validation. A moderately thick square ($a \times a$ and $a/h = 10$) simply supported cross-ply laminated plate is analyzed for two different constructions, 2 ply (0/90) and 4 ply ($0°/90°/0°/90°$), where a is the side and h is the thickness. A transverse uniformly distributed mechanical load (w) is applied. Material properties used are $Y_{11}/Y_{22} = 25, G_{12}/Y_{22} = 0.5, G_{13}/Y_{22} = G_{23}/Y_{22} = 0.2, \nu_{12} = 0.25$. The following dimensionless quantities are considered, central deflection (w/h) and load ($qa^4/Y_{22}h^4$). The load-deflection curve is plotted and compared with the analytical solution results given in [45]. Figure 2.10 shows that the developed finite element model is in good agreement with the analytical solution results. Also, we can notice here that for the same side to thickness ratio (a/h), 4 ply composite plate has less deflection than that of 2 ply plate.

In order to verify the finite element model for the static mechanical loading case, an all-clamped four ply ($0°/90°/90°/0°$) square plate having dimensions $a = b = 12$ in, $h = 0.096$

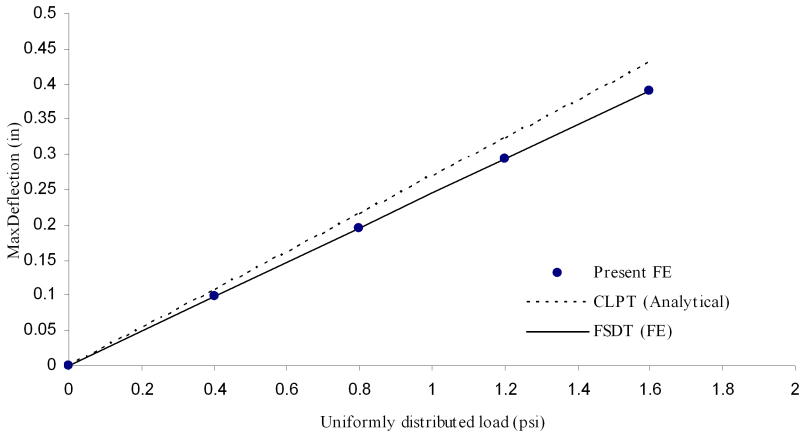

Figure 2.11: Static deflection with distributed load

in, with a uniformly distributed load q_0 was modeled. The maximum center deflection is shown in Figure 2.11 against the increasing load and its comparison with classical laminated plate theory (CLPT) [53] and first-order shear deformation theory (FSDT)[12]. The finite element results were in very good agreement with the theoretical results. The material properties used here are: Y_{11}= 1.8282 x 10^6 psi, Y_{22}= 1.8315 x 10^6 psi, $G_{12} = G_{13} = G_{23}$ = 0.3125 x 10^6 psi, and Poisson's ratio= 0.23949.

Chapter 3

Composite Plates with Piezoelectric Patches

Structures which can sense and react according to the action of their surroundings are called smart structures. In general, smart structures consist of a sensing unit, which sense the action, and an actuation unit to generate response, and finally a control unit to monitor and control the entire process. The actuation and sensing are often achieved by employing materials with special properties called smart materials. Smart materials have the ability to convert one form of energy into another that can be eventually used in sensing or in actuation. Different types of materials have been tested and used successfully in smart sensing and actuation, depending upon the applications. Piezoelectric materials, shape memory alloys, magnetorheological fluids and magnetostrictive materials are among these materials. Piezoelectric materials are widely used in structural applications such as shape control, vibration control, and micro-positioning due to their direct coupling between electrical and mechanical fields, high stiffness, and fast frequency response and their very high achievable strain rate when compared to other materials.

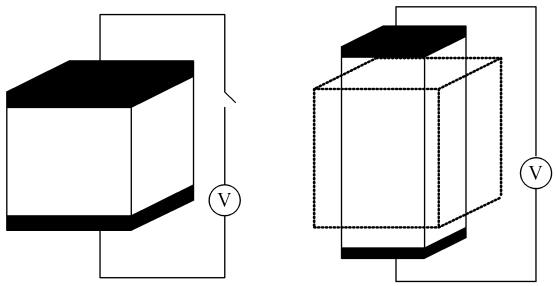

Figure 3.1: Schematic representation of piezoelectric effect

This chapter briefly discusses the fundamentals of piezoelectric materials, their constitutive relations and modeling of piezoelectric patches in composite plates with the finite element procedure. Review of the hysteresis models for piezoelectric materials and their implementation is also addressed in this chapter. The self-sensing actuator concept, used to achieve truly collocated actuator/sensor pairs is discussed at the end.

3.1 Fundamentals of piezoelectricity and piezoelectric materials

The piezoelectric effect can be seen as a direct coupling between electrical and mechanical fields. This is of two types, one is the direct piezoelectric effect and the other is the converse piezoelectric effect. Piezoelectric crystal produces mechanical displacement (strain) under an electrical field. This property is termed the converse effect. The production of electric field due to mechanical strain is termed the direct effect. Figure 3.1 shows the converse effect schematically. The direct piezoelectric effect was observed by Curie brothers (Pierre Curie, Jacques Curie) in 1880 in some natural crystals like cane sugar, and in Rochelle salt [39]. They also verified the inverse piezoelectric effect in 1881. Some of its applications such as sonar, ultrasonic, microphone and transducers came to use during the first and second

world wars [39]. For a material to exhibit anisotropic properties such as piezoelectricity, its crystal structure must have no center of symmetry [8]. Among the naturally available crystals, 21 classes of crystals out of 32 are non-centro symmetric. Out of them, 20 classes of crystals show piezoelectric effect. The different modes of piezoelectric effects seen in natural crystals are the longitudinal, transverse, longitudinal shear and the transverse shear. Three possible electric fields and six possible strains make the piezoelectric coefficient matrix $d_{h,k}$ of size 3x6. The non-zero components in the piezoelectric coefficient matrix and the direction of applied electric field decide the mode of deformation.

The transverse mode is the most common mode of actuation in structural applications such as surface bonded or embedded actuators/sensors. These actuators when polarized in the thickness direction produce a deformation along the axis of the substrate; the resultant is a couple about the center-line of the substrate. In the sensor case the reverse is true. The materials used in this work are such that they have dominant d_{31} coefficients, and if they are applied with electric potential in thickness direction(3) they deform more in longitudinal direction(1) and is used in bending applications. The longitudinal effect is used in point actuators, where the extension takes place in the longitudinal direction. The shear effect also has been occasionally used in strain actuation applications [5]. The piezoelectric effect exhibited by natural crystals such as quartz, Rochelle salt etc, is very small, costly and their availability in the desired size and shape is very limited [13]. Hence, synthetically-developed piezo-ceramics and piezo-polymers have been widely used in smart structure applications in recent years [13]. PZT (lead-zirconate titanate), a ceramic, and PVDF (polyvinylidene fluoride), a polymer, are very popular among them. Poling is a process that aligns the random domains along the polarization direction; it is achieved by applying a strong DC voltage in one direction on the heated PZT. During poling the material permanently increases dimensionally along the poling direction and reduces in other

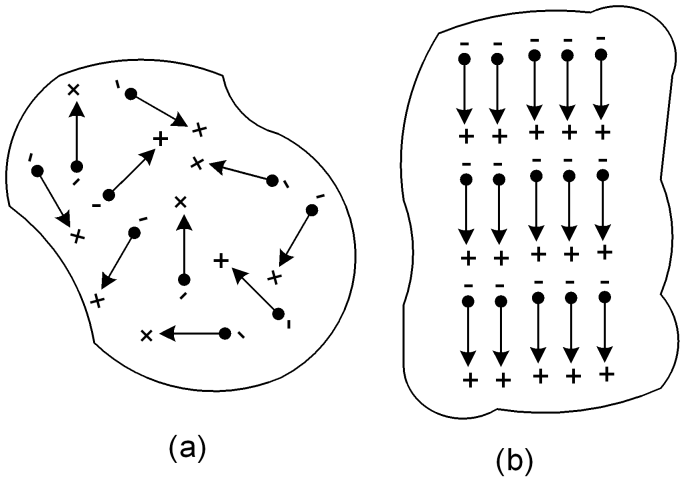

Figure 3.2: Dipoles in PZT before and after poling

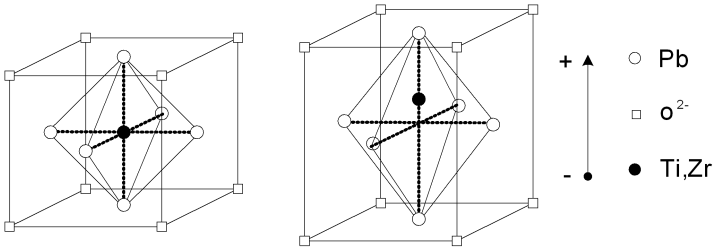

Figure 3.3: Unit cell of PZT before and after polling

direction (Figure 3.2b). The atomic structure of PZT is given in Figure 3.3, before and after poling along with the poling direction. PZT ceramics have anisotropic structure after poling below the *Curie temperature* above which they loose their piezoelectric properties. The dipole behavior of this material is due to the charge separation between the positive and negative ions. The Weiss domains (ferroelectric domains), a group of dipoles with parallel orientation, are randomly oriented in the PZT before poling (Figure 3.2a).

The use of piezoelectric actuators as elements of intelligent structures was successfully demonstrated by Crawley and Louis in [13]. They presented analytical and experimental development of structures with distributed actuators and sensors. They demonstrated

with beam-like structures having surface bonded or embedded actuators. Large flexible structures such as antennas, mirror, and aircraft wings etc are generally made of composite materials and their shape and vibration control problems were studied by many researchers by using the piezoelectric material layers or patches as the actuating and sensing elements [9, 12, 14, 20]. The next sections discuss the constitutive relations for a piezoelectric lamina for which actuator and sensor equations are derived. The finite element model developed in the previous chapter for composite plates is modified to include the piezoelectric material layers and piezoelectric patches.

3.2 Modelling of piezoelectric lamina

A piezoelectric lamina is a layer of piezoelectric martial. Its linear constitutive equations coupling the elastic and electric fields can be written for a plane stress reduced condition as [50]

$$\begin{aligned} \{\sigma\} &= [\bar{Q}]\{\epsilon\} - [\bar{e}]^T\{E\} \\ \{\mathcal{D}\} &= [\bar{e}]\{\epsilon\} + [\bar{p}]\{E\} \end{aligned} \tag{3.1}$$

with

$$[\bar{e}] = [\bar{Q}]\{\bar{d}\}$$

where $\{\sigma\} = [\sigma_{xx}, \sigma_{yy}, \sigma_{xy}, \tau_{yz}, \tau_{xz}]^T$ is the elastic stress vector and $\{\epsilon\} = [\epsilon_{xx}, \epsilon_{yy}, \epsilon_{xy}, \gamma_{yz}, \gamma_{xz}]^T$ is the elastic strain vector, $\{E\}$ is the electric field vector, $\{\mathcal{D}\}$ is the electric displacement vector (a measurable quantity equal to the charge per unit area of an electrode), $[\bar{Q}]$ is the transformed elastic constitutive matrix and $[\bar{e}]$ is the transformed piezoelectric stress coefficients matrix, $[\overline{p}]$ is the transformed dielectric constants matrix and $[\overline{d}]$ is the transformed

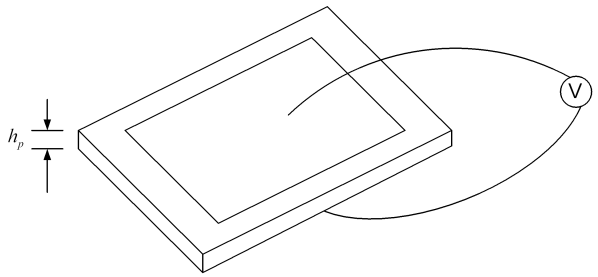

Figure 3.4: Piezoelectric lamina with surface electrode

piezoelectric strain coefficient matrix in the local coordinate system (x, y, z) of the lamina using the ply angle of the lamina α (see Figure 2.4). The transformation of vectors and matrices from the material axes system (x_1, x_2, x_3) to local system (x, y, z) of the lamina and the coefficient matrices are given in Appendix A. The first equation of (3.1) represents the converse effect and hence it is used in actuator designs. The second one governs the direct effect and is used in sensor designs.

Piezoelectric actuators are available in different shapes, such as rod, plate etc. The rod type actuators, polarized in the longitudinal direction, are used as stacked actuators in point actuation. The plate type actuators polarized in thickness direction are used in distributed actuation on plate and shell-like structures. They have electrodes on both sides, Figure 3.4. The electric field vector $\{E\}$ is the negative gradient of the applied electric potential V, the voltage applied in the thickness direction. i.e.,

$$\{E\} = - \bigtriangledown V \tag{3.2}$$

where

$$\{E\} = \{0, 0, E_z\}^T$$

and

$$E_z = -V/h_p$$

where h_p is the thickness of the piezoelectric layer. The actuator equation is derived from the induced strain actuation definition of equation (3.1) with no applied stress in the piezoelectric layer. From equation (3.1), stresses due to the applied electric field, $\{\sigma_p\}$, in the piezoelectric layer is

$$\{\sigma_p\} = [\bar{e}]^T\{E\}$$

where $\{\sigma_p\}$ can be related to the the strain in the piezoelectric layer $\{\epsilon_p\}$ as

$$\{\sigma_p\} = [\bar{Q}]\{\epsilon_p\}.$$

Therefore the strain can be related to the electric field using the above two relations as

$$\{\epsilon_p\} = [\bar{Q}]^{-1}[\bar{e}]^T\{E\}. \tag{3.3}$$

By using equation (3.3) and the general strain definition (2.3) the total strain vector $\{\epsilon\}_{tot}$ for electro-elasticity can can be written as

$$\{\epsilon\}_{tot} = \left\{ \begin{array}{c} \{\epsilon\} \\ \{\epsilon_p\} \end{array} \right\} = \left\{ \begin{array}{c} \{\epsilon\}^l + \{\epsilon\}^{nl} \\ \{\epsilon_p\} \end{array} \right\} \tag{3.4}$$

where $\{\epsilon\}$ is the elastic strain given by the equation (2.3). This expression for strain is used in the general nonlinear constitutive model of the smart structures with actuators.

The sensor equation can be derived from the second equation of the electro-elastic relation of a piezoelectric lamina (equation (3.1)). The electric displacement in the thickness

direction can be written as

$$\mathcal{D}_z = e_{31}\{\epsilon\}$$

where e_{31} is the dominant piezoelectric constant. The total charge $\mathsf{q}(t)$ developed on the sensor surface is the spatial summation of all the point charges and can be calculated by integrating the electric displacement over the sensor surface area as

$$\mathsf{q}(t) = \int_S \mathcal{D}_z dS \tag{3.5}$$

where S is the surface area of the sensor. The open circuit sensor voltage output from the sensors can be written as:

$$\phi_s(t) = G_c i(t) \tag{3.6}$$

where G_c is the gain of the current amplifier. The current $i(t)$ on the sensor is the time derivative of the total charge and can be written as

$$i(t) = \frac{d\mathsf{q}(t)}{dt} \tag{3.7}$$

where $\mathsf{q}(t)$ is the total charge given by equation (3.5).

3.3 Finite element implementation of piezoelectric patches

A piezoelectric patch is either surface bonded or embedded into the substrate composite plate to form piezolaminated composites. The bond between the layers is assumed to be perfect so that the displacement remains continuous across the bond. The layered composite plate with piezoelectric layer modeled in [45], is modified to include the transverse piezoelectric force resultant. Piezoelectric force, moment and transverse force resultants

per unit length are denoted by $\{N^p\}, \{M^p\}$ and $\{T^p\}$, respectively. They can be written as:

$$\{N^p\} = \left\{ \begin{array}{c} N^p_{xx} \\ N^p_{yy} \\ N^p_{xy} \end{array} \right\} = \sum_{k=1}^{n_p} \int_{z_k}^{z_{k+1}} [\bar{e}]^k \{E\}^k \, dz,$$

$$\{M^p\} = \left\{ \begin{array}{c} M^p_{xx} \\ M^p_{yy} \\ M^p_{xy} \end{array} \right\} = \sum_{k=1}^{n_p} \int_{z_k}^{z_{k+1}} [\bar{e}]^k \{E\}^k \, z dz, \tag{3.8}$$

$$\{T^p\} = \left\{ \begin{array}{c} T^p_x \\ T^p_y \end{array} \right\} = \mathrm{s} \sum_{k=1}^{n_p} \int_{z_k}^{z_{k+1}} \left[\begin{array}{ccc} \bar{e}_{14} & \bar{e}_{24} & 0 \\ \bar{e}_{15} & \bar{e}_{25} & 0 \end{array} \right]^k \{E\}^k dz,$$

where n_p represents the number of piezoelectric layers. The addition of piezoelectric material into the composite (substrate) changes the force and moment resultants (equation (2.10)) as follows

$$\left\{ \begin{array}{c} \{N\} \\ \{M\} \\ \{T\} \end{array} \right\} = \left[\begin{array}{ccc} [A_{ij}] & [B_{ij}] & 0 \\ [B_{ij}] & [D_{ij}] & 0 \\ 0 & 0 & \mathrm{s}[S] \end{array} \right] \left\{ \begin{array}{c} \{\epsilon_p\} \\ \{\epsilon_b\} \\ \{\epsilon_s\} \end{array} \right\} - \left\{ \begin{array}{c} \{N^p\} \\ \{M^p\} \\ \{T^p\} \end{array} \right\}$$

where matrices $[A], [B], [D]$ and $[S]$ are as given in equation (2.10).

Finite element modelling of piezoelectric materials and layered composites with piezoelectric layers were presented in the literature over the years. A three-dimensional finite element was developed and presented in [20, 57] for the analysis of piezoelectric continuum. Laminated plate elements with piezoelectric layers using classical plate theory is presented in [14, 24, 32]. Nonlinear finite element modeling of laminated plates were presented in

[51, 55], they follow the same formulation presented in [46] for isotropic plates. Nonlinear finite element analysis of laminated composites with piezoelectric actuators/sensors is one area which is less reported in the literature. A 20 node brick element for modelling piezoelectric continuum is presented in [61]. Solid elements are not efficient for modeling plate structures due to the shear locking (a phenomenon characterized by a severe underestimation of the displacements [50]) when used to model the plate structures. Also a large number of elements are required to get reasonable results. Another non-linear finite element based on classical laminate theory for piezoelectric laminated plate is presented in [41]. Recently, other methods such as an element-free Galerkin method [37] are used in the analysis of these structures. Commercially available finite-element analysis packages such as ANSYS, ABAQUS have piezoelectric capabilities in their finite elements solid and plate elements. They are useful for modeling the piezoelectric transducers (piezoelectric structures) rather than modeling structures with integrated piezoelectric patches. Non-linear electro-mechanical capabilities are not considered in their modeling as such but an user written sub-routines can be used to include the non-linearity. Layered composite plate elements with piezoelectric capabilities are not available in their element library. In this thesis an efficient finite element plate model with shear deformation is presented for modeling thick layered composite plates with bonded piezoelectric actuators, including self-sensing capabilities and nonlinear electro-mechanical effects.

In order to model the piezoelectric patches, the element developed in Section 2.3 is used with one electrical degree of freedom per layer added to the five displacement degrees of freedom. The electric potential is assumed to be constant over an element and varying linearly through the thickness [32]. The total strain given in equation (3.4) is used in deriving the element matrices. A special numbering scheme is used to denote the elements with piezoelectric patches. Elements with piezoelectric patches are denoted with 1 and

others have 0 for the identification during the assembly process. The finite element equation (equation (2.23)) developed for a layered composite plate from the energy principles is modified to include the piezoelectric resultants as:

$$\begin{bmatrix} M_{uu} & 0 \\ 0 & 0 \end{bmatrix} \begin{Bmatrix} \{\ddot{u}\} \\ 0 \end{Bmatrix} + \begin{bmatrix} K_{uu} & K_{u\phi} \\ K_{\phi u} & K_{\phi\phi} \end{bmatrix} \begin{Bmatrix} \{u\} \\ \{\phi\} \end{Bmatrix} = \begin{Bmatrix} \{F\} \\ 0 \end{Bmatrix}, \tag{3.9}$$

where $[K_{uu}]$ is the elastic stiffness matrix, $[K_{\phi\phi}]$ is the electric stiffness matrix and $[K_{\phi u}]$, $[K_{u\phi}]$ are the coupling matrices. Actuator and sensor equations can then be written as:

$$\{u\} = [K_{uu}]^{-1}(\{F\} - [K_{u\phi}]\{\phi_A\} \tag{3.10}$$

$$\{\phi_S\} = -[K_{\phi\phi}]^{-1}[K_{\phi u}]\{u\} \tag{3.11}$$

where $\{\phi_A\}$ and $\{\phi_S\}$ are electric displacement vectors of actuation and sensing.

The global dynamic equation after assembly becomes,

$$[M]\{\ddot{u}\} + ([K_{uu}] - [K_{u\phi}][K_{\phi\phi}][K_{\phi u}])\{u\} = \{F\} - [K_{u\phi}]\{\phi_A\}.$$

The stiffness matrix definitions are given in Appendix B.

3.4 Hysteresis modeling in piezoelectric materials

In ferroelectric materials during poling (Section 3.1) the dipoles which are aligned to the applied field grow and others shrink, so that there is no net strain, but with sufficiently large field some dipoles switch directions and there is now a net piezoelectric effect. As a result, domain walls (an imaginary wall separating neighboring domains with differently

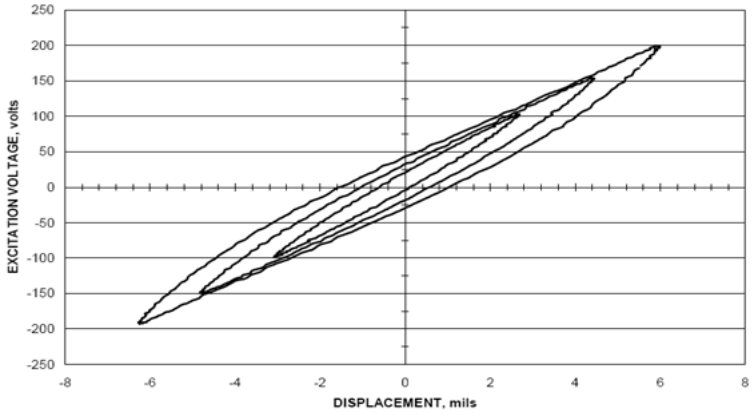

Figure 3.5: Typical hysteresis loop for piezoelectric material

oriented dipoles) will move. The domain walls are said to move corresponding to the applied electric field, however the material dislocation defects interact with the dipoles and obstruct the domain wall movement by pinning [23]. The unrecoverable energy loss occurring in the applied field to overcome domain wall pinning is believed to be the primary source of hysteresis in ferroelectric materials [23]. Hysteresis in piezoelectric materials is a concern in shape control and micro-positioning applications where accuracy plays a major role. Hysteresis is due to the ferroelectric nature of piezoelectric elements. For piezoelectric materials, the hysteresis increases when the peak voltage is increased. Figure 3.5 shows a typical hysteresis loop [27].

One of the very popular hysteresis models is the Preisach model and it is widely used for magnetic materials. Ge and Jouaneh [18] and Hughes *et al* [23] used a Preisach model to study the hysteretic behavior of piezoelectric actuators, this model was earlier used for magnetic materials by Doong and Mayergoyz [15]. The results were verified with an experiment conducted on stacked actuators with periodic sinusoidal and triangular input voltages. Another approach given by Ralph C. Smith [56], the homogenized energy model,

is a flexible and efficient macroscopic model for ferroelectric materials. Other notable models for piezoelectric hysteresis available in the literature are the Jiles-Atherton model [17], a macroscopic theory given by Chen and Mongomery [11] and an implicit algorithm for predicting the hysteresis behavior of piezoelectric actuators presented by Leigh and Zimmerman [34].

3.4.1 Energy model for piezoelectric materials

In the homogenized macroscopic polarization model [56], the polarization is expressed as

$$[P(E)](t) = \int_0^\infty \int_{-\infty}^\infty \nu_1(E_c)\nu_2(E_I)[\overline{P}(E + E_I;\ E_c, \xi)](t) dE_I dE_c \tag{3.12}$$

where ξ denotes the initial distribution of dipoles. E is the electric field and E_c is coercive field which reduces the polarization to zero and is given by

$$E_c = \eta(P_R - P_I)$$

where P_R is reversible and P_I is irreversible polarizations. E_I denotes the interaction field due to neighboring dipoles as well as certain electromechanical interactions. The functions $\nu_1(E_c)$ and $\nu_2(E_I)$ denotes general densities. A priori choice for densities is[56]

$$\begin{aligned} \nu_1(E_c) &= c_1 e^{-[\ln(E_c/\bar{E}_c)/2c]^2} \\ \nu_2(E_I) &= c_2 e^{-\frac{E_I^2}{2b^2}} \end{aligned}$$

where $c_1 \cdot c_2 = C$, and the approximate value $\langle E_c \rangle = \bar{E}_c$ are used to obtain the initial parameter estimates. This formulation requires the identification of five parameters $\eta, \bar{E}_c, c, b$

and $c_1 \cdot c_2 = C$. All of these coefficients can be qualitatively interpreted [56]. The local average polarization $\overline{P}$ is obtained through the minimization of the Gibbs energy

$$G(E, P, T) = \psi(P, T) - EP$$

where $\psi(P, T)$ represents the Helmholtz energy. The kernel resulting from the the Helmholtz energy expression has the form

$$\overline{P}(E) = \frac{1}{\eta} E + P_R \delta$$

where $\delta = -1$ for negatively oriented dipoles and $\delta = 1$ for those with positive orientation. A discretized version of this model for numerical implementation, based on Gaussian-Legendre quadrature rule, is also presented in [56].

3.4.2 Implementation in FEM

The implementation of the hysteresis model into a finite element model is important as finite element models are widely used in the study of smart structures. The literature on the inclusion of hysteresis into finite element models is limited. Marc Kamalah *et al* [31] discussed a macroscopic constitutive law for ferroelectric and ferroelastic hysteresis effect of piezo-ceramics and their implementation in finite element modelling. An elastically linear beam finite element model was developed by Paul *et al* [44] to model the optical beams with bending actuators. This model includes the hysteresis effect by adding the polarization term into the constitutive equation (3.1) as

$$\{\sigma\} = [\overline{Q}]\{\epsilon\} - [\overline{e}]^T\{E\}$$

$$\{\mathcal{D}\} = [\overline{e}]\{\epsilon\} + [\overline{p}]\{E\} - \alpha_1 P \tag{3.13}$$

where P is the polarization. The electric field change due to a unit polarization is denoted by α_1. Ralph C. Smith [56] has given a numerical implementation of homogenized energy model into a finite element model. The constitutive relation for one-dimensional case was obtained from the polynomial energy expression as:

$$\sigma \;\; = \;\; Y^P \epsilon - a_1 P - a_2 P^2 \tag{3.14}$$

where the Young's modulus at constant polarization is denoted by Y^P, a_1 and a_2 are positive coupling coefficients and P is the polarization obtained by the homogenized energy model [56]. In order to implement this model in the finite element developed here (Section 3.3), the constitutive equation (3.14) is used to calculate the piezoelectric force and moment resultants. Equation (3.8) is re-written as,

$$\begin{aligned}
\{N^p\} &= \sum_{k=1}^{n_p} \int_{z_k}^{z_{k+1}} ([\overline{e}]^k \{E\}^k - \alpha_1 P^k) dz \\
\{M^p\} &= \sum_{k=1}^{n_p} \int_{z_k}^{z_{k+1}} ([\overline{e}]^k \{E\}^k - \alpha_1 P^k) z dz \\
\{T^p\} &= \mathrm{s} \sum_{k=1}^{n_p} \int_{z_k}^{z_{k+1}} \left(\begin{bmatrix} \bar{e}_{14} & \bar{e}_{24} & 0 \\ \bar{e}_{15} & \bar{e}_{25} & 0 \end{bmatrix}^k \{E\}^k - \alpha_1 P^k \right) dz
\end{aligned}$$

in order to include the polarization. P^k was calculated by using the discretized macroscopic model (Equation (3.12)) for each piezoelectric layer k. This model needs to be added and tested in the developed finite element code in this thesis.

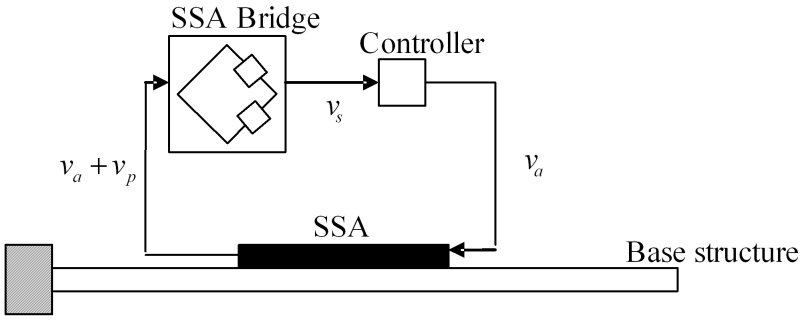

Figure 3.6: Schematic diagram of self-sensing actuator

3.5 Self-sensing actuators

Self-sensing actuation is a technique which uses a single piece of piezoelectric material for sensing and actuation concurrently in a closed loop system [16]. Figure 3.6 represents the schematic of self sensing actuator functions. Self-sensing actuators are truly collocated and hence the resulting control system has all the desirable properties of collocated control systems such as symmetric transfer functions, and this has been shown to provide greater advantages in stability, passivity, robustness and in implementation [4]. In the case of separate actuators and sensors, the maximum benefit can be achieved by having them placed in close proximity. Self-sensing eliminates the possible closed loop control problems arising from the capacitive coupling between the sensors and actuators [16]. Another advantage in using self-sensing is the reduced number of piezoelectric elements required for any application.

Dosch *et al* [16] developed a theoretical basis for self-sensing actuators in terms of the electro-mechanical constitutive equations for piezoelectric material. Yellin and Shen [63] used the self-sensing actuator in active constrained layer damping treatment of a beam. Finite element implementation of self-sensing actuator concept into a first order theory

based plate element is discussed by Chang-Qing *et al* [10]. The sensor equation (3.11) can be written as:

$$\{\phi_S\} = -\beta[K_{\phi\phi}]^{-1}[K_{\phi u}]\{\phi_A\} \tag{3.15}$$

where β is a constant obtained from the bridge circuit, $[K_{\phi\phi}]$ and $[K_{\phi u}]$ are stiffness matrices and $\{\phi_A\}$ is actuator voltages . The equivalent piezoelectric sensor's capacitance used to separate the sensor voltage is an unknown and its matching is a major problem. Pourboghrat *et al* [47] presented an adaptive method for the on-line estimation of the equivalent capacitance for layered self-sensing actuator. They have also used a simple PID controller for the vibration reduction and motion control applications of a cantilever beam. Implementation of self-sensing actuator for vibration control of structures with adaptive mechanisms is reported in [33, 36]. The main difficulty in using self-sensing actuators is obtaining a clean self-sensing signal due to the input voltage dependent piezoelectric capacitance. Linear piezoelectric capacitance relation is used to model the dependency [26]. Recently an extrinsic Fabry-Perot interferometer is used with piezoceramic[PZT] to obtain a self-sensing mechanism to avoid the difficulties caused by the nonlinear piezoelectric capacitance and phase error [9].

3.6 Numerical simulation

Numerical simulations using the developed finite element model are done on composite plates with linear piezoelectric patches on them. First, static shape control application is done in order to verify the piezoelectric modelling in the code. A simply supported four layer composite (T300/976 unidirectional graphite/epoxy composite) plate with two additional actuator layers (PZT G1195N) at the top and bottom of the plate $[P/-30^\circ/30^\circ/30^\circ/-30^\circ/P]$ is modeled with a uniformly distributed load of 50 N/m^2,

Table 3.1: Materials properties

	PZT G-1195	T300/976
Y_{11} GPa	63	150
Y_{22} GPa	63	9
ν	0.29	0.3
G_{12} GPa	24.8	7.1
G_{13} GPa	-	7.1
G_{23} GPa	-	2.5
Density kg/m^3	7600	1600
d_{31} pm/V	-166	-
d_{32} pm/V	-166	-

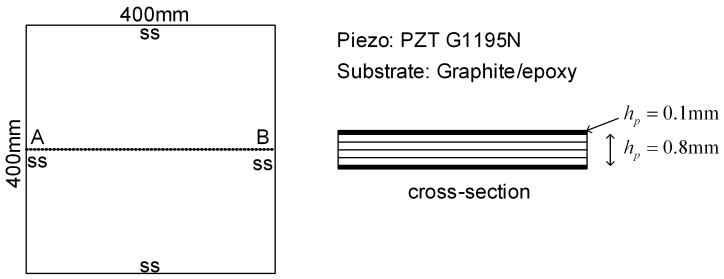

Figure 3.7: Plate geometry

with different electric potential. The plate dimensions considered are: $a = b = 400$ mm and total thickness $h = 0.8$ mm and the thickness of piezoelectric layers is 0.1 mm. The material properties considered are in Table 3.1 . Figure 3.7 shows the plate considered here with the dimensions and boundary conditions. It is assumed that all the elements have a piezoelectric material layer. The center line (line-AB in Figure 3.7) deformation obtained is given in Figure 3.8 for various input electric potentials.

In order to show the efficiency of the plate finite element the present code is compared with commercial finite element software. ANSYS, ABAQUS and NASTRON are some of the commercially available software that have electro-mechanical analysis capabilities. ABAQUS is selected among them for the comparison because of its ease of use with input

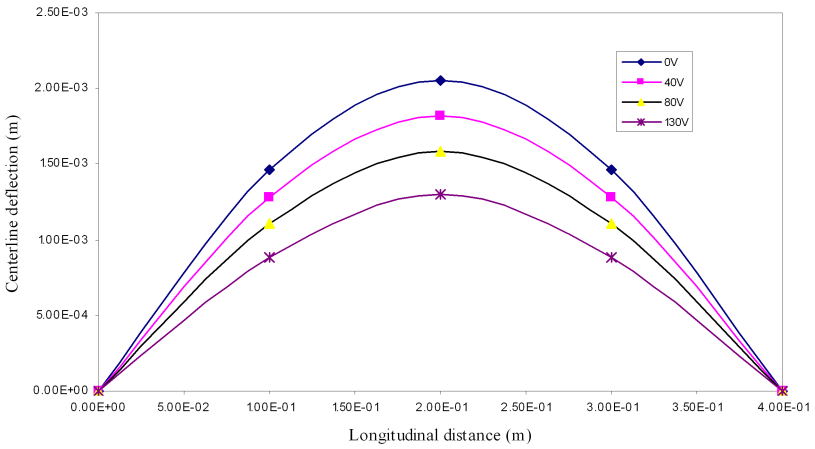

Figure 3.8: Static shape control of composite plate

files and strong multi-physics capabilities. For this comparison an annular aluminum plate with selectively bonded piezoelectric patches as shown in Figure 3.9 is considered and it is modeled with the Matlab code devoleped here and also with solid elements in ABAQUS. The plate is clamped along the inner edge and a 55V electric potential is applied.

The plate model is meshed with three different number of elements using the Matlab code developed. The total number of element (NEM) and the total number of nodes (NNM) in the mesh along with the results are summarized in the Table 3.2 for the three models. Figure 3.10 shows the meshing used in the Matlab code with 180 elements. The undeformed and deformed shape of the plate obtained from the Matlab code is shown in Figure 3.11 . A convergence study is performed using the code with increasing number of elements and the results are tabulated (Table 3.2) and the deflection along the line-AB(Figure 3.9) is given in Figure 3.12. From the figure it is clear that increasing the number of plate elements does not make significant change to the converged results. The

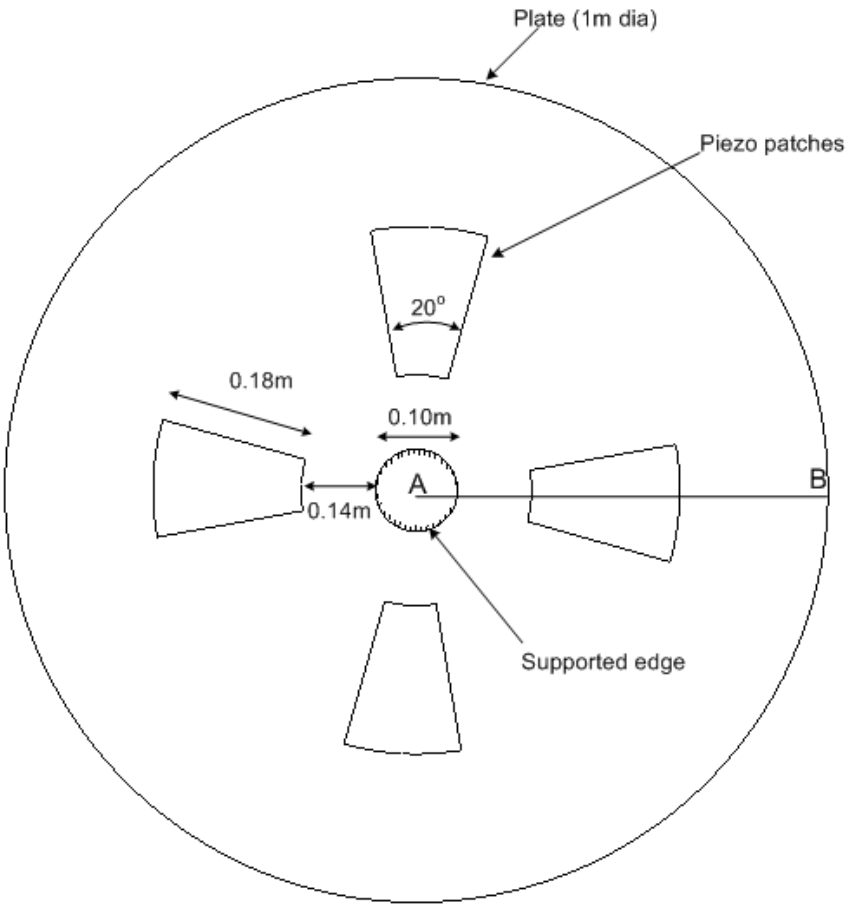

Figure 3.9: Clamped annular plate with piezoelectric patches - geometry

Table 3.2: Convergence with plate element

Model	NEM	NNM	End deflection(m) (point-B)
MP1	180	216	4.47×10^{-4}
MP2	720	792	4.38×10^{-4}
MP3	2880	3024	4.37×10^{-4}

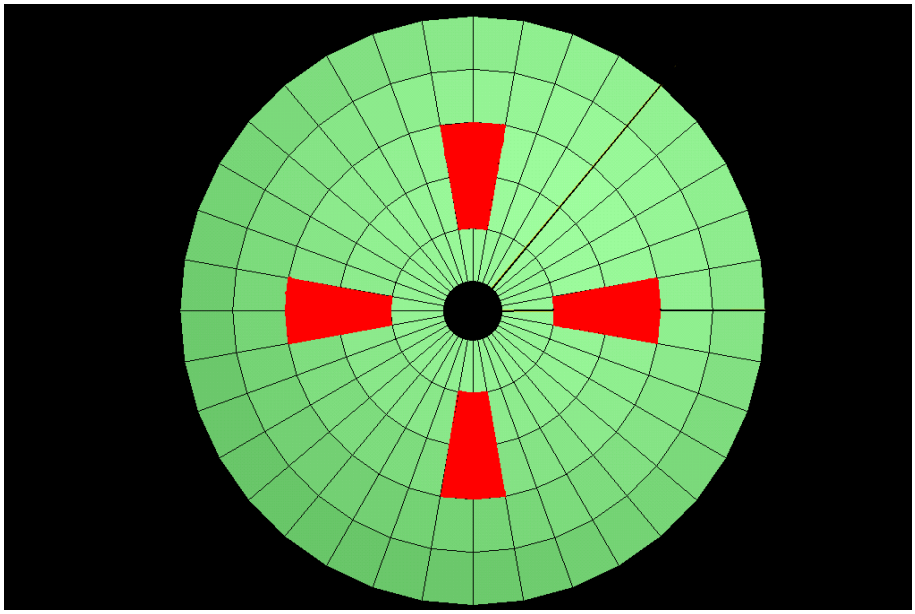

Figure 3.10: Clamped annular plate with piezoelectric patches - mesh

CPU time taken to run the model (with 180 elements) using Matlab code on an AMD Athlon 64x2 processor workstation was reported as 8.4063 sec, this was calculated utilizing the 'cputime' function in Matlab.

Similar convergence study is performed using four different model with increasing number of solid elements in ABAQUS and the results obtained are tabulated (Table 3.3). Figure 3.13 shows the deflection along line-AB. From Figure 3.13 and Table 3.3 it is clear that a large number of solid elements are required to obtain convergence. The CPU time taken to run a model (with 1970 elments) using solid elements in ABAQUS on an AMD Athlon 64x2 processor workstation was reported as 15.2011 sec. The comparison of the converged results from the Matlab code and ABAQUS is given in Figure 3.14. This result validates the developed finite element code and also shows the efficiency of it over the commercial software.

Table 3.3: Convergence with solid element in ABAQUS

Model	NEM	NNM	End deflection(m) (point-B)
MS1	1970	4684	3.61×10^{-4}
MS2	2884	5984	3.98×10^{-4}
MS3	15430	31260	4.378×10^{-4}
MS4	35058	70716	4.37×10^{-4}

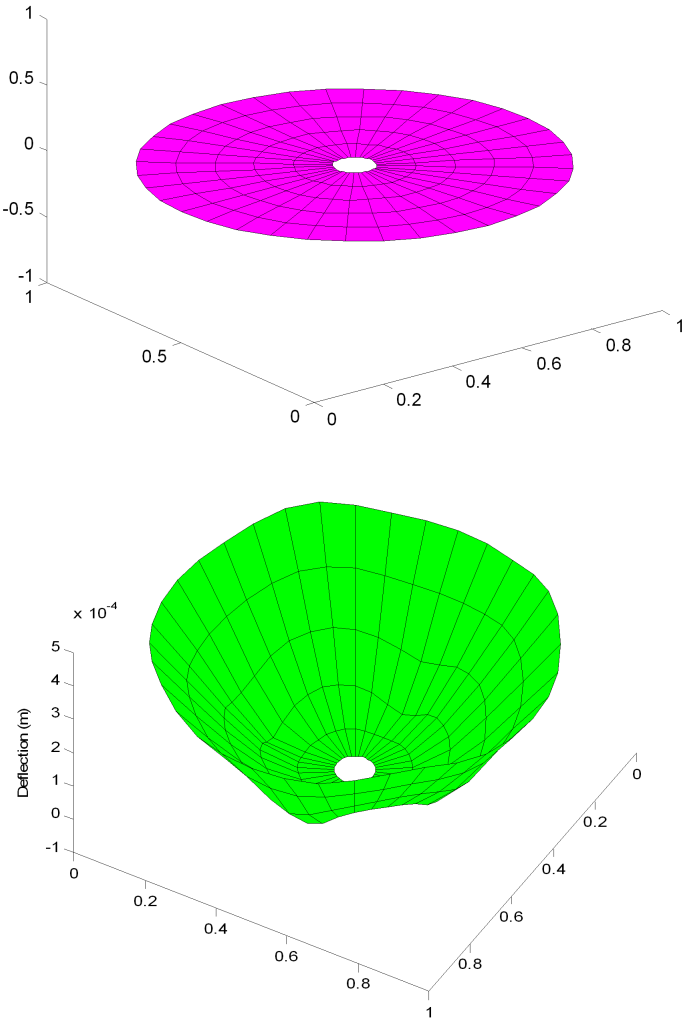

Figure 3.11: Plate code results-undeformed and deformed shape of the plate

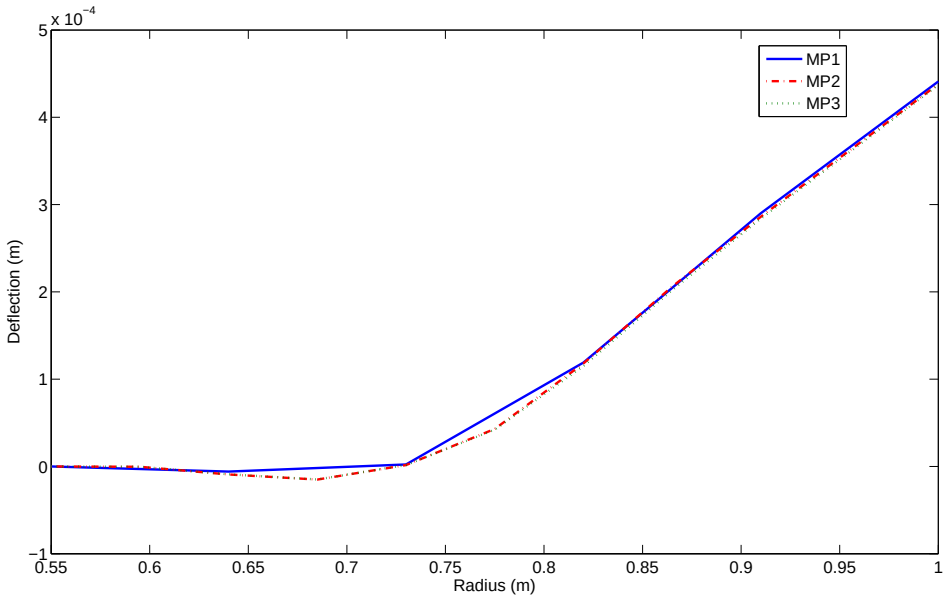

Figure 3.12: Convergence with plate elements

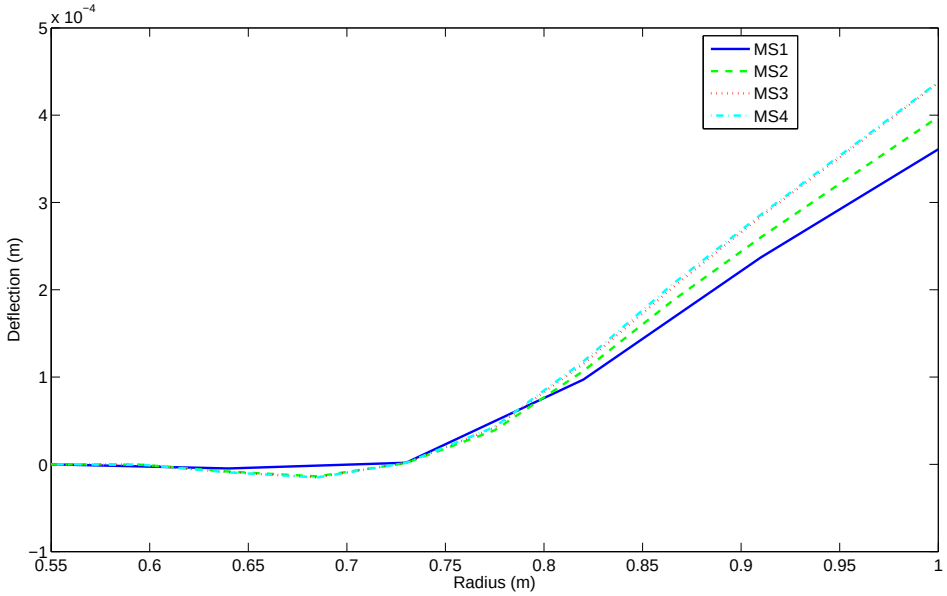

Figure 3.13: Convergence with solid element in ABAQUS

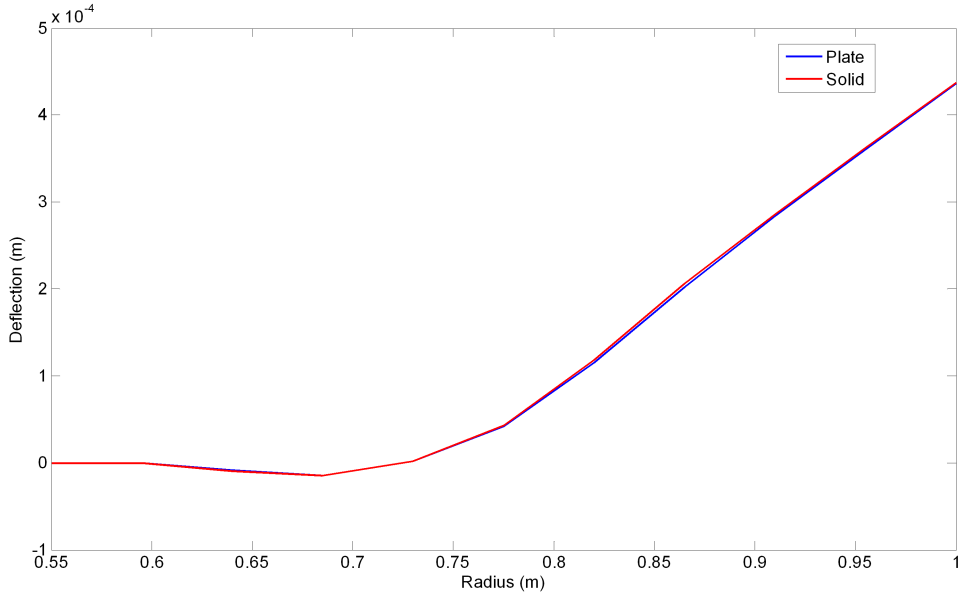

Figure 3.14: Comparison of code and ABAQUS results

Chapter 4

Optimal locations of actuators/sensors

Active structures can be controlled effectively, that is, a desired shape can be achieved by using segmented piezoelectric actuators/sensors (piezoelectric patches) rather than having actuators/sensors distributed over the structure[13]. Segmented actuators/sensors give more flexibility than the actuators distributed all over the structure in operation because the voltage applied to individual actuators can be controlled. They can be placed where they can be most effective. Placement of actuators and sensors at appropriate locations is an important factor in smart structure design in order to achieve the desired shape statically or dynamically and also for vibration control of structures. In this chapter all studies are based on piezo actuators with linear model and no hysteresis

4.1 Dynamic shape control

In dynamic shape control, poorly placed actuators and sensors may cause lack of observability and controllability or poor system performance [2]. Finding optimal placement of actuators and sensors together with optimal control parameters, such as controller gain,

is approached in different ways in the literature. In this chapter, different strategies used to form the objective functions used for this problem are discussed. The use of different objective functions to find the optimal location of an actuator is also discussed and numerical examples are given. A finite element model is used to find an optimal location for linear-quadratic control on a beam.

4.1.1 Strategies for optimal location

The placement of actuators/sensors is done mainly based on two different criteria, (1) controllability and observability measures and (2) linear quadratic controller design. Placement based on controllability will be discussed first. The basic concept here is to consider this optimization problem as a minimum control energy problem. Consider a second order system,

$$M\ddot{q} + \mathcal{C}\dot{q} + Kq = Fu \tag{4.1}$$

where M is the mass matrix, $\mathcal{C}$ is the damping matrix, K is the stiffness matrix, F is the force vector, q is the vector of displacement and u is the input vector. This system can be written as a linear state-space model

$$\begin{aligned} \dot{x} &= \mathsf{A}x + \mathsf{B}u \\ y &= \mathsf{C}x \end{aligned} \tag{4.2}$$

where $x = \{q, \dot{q}\}^T$ is the state vector, u is the input and y is the output vectors respectively. The system matrices A and B are defined as follows:

$$\mathsf{A} = \begin{bmatrix} 0 & I \\ -[M]^{-1}[K] & -[M]^{-1}[\mathcal{C}] \end{bmatrix}$$
$$\mathsf{B} = \begin{bmatrix} 0 \\ [M]^{-1}[F] \end{bmatrix} \tag{4.3}$$

and C is the observation matrix.

System (4.3) is *controllable* if for any initial condition x_0, final condition x_f, and time $t_f > 0$, there exists a piecewise continuous input u so that $x(t_f) = x_f$ [42]. The actuators could be placed at some desired locations in order to bring the system to the final state $x(t_f) = x_f$ with minimal control energy. This can be achieved by considering the following minimum energy problem [30],

$$J = \min_u \int_0^{t_f} u^T(t)u(t)dt \tag{4.4}$$

subject to the the system dynamics (equation (4.2)) with given initial and final conditions. This linear quadratic optimal control problem with fixed final time and state has an optimal solution [28]

$$u_0(t) = -\mathsf{B}^T e^{\mathsf{A}(t_f - t)} W^{-1}(t)(e^{\mathsf{A}t_f}x_0 - x_{t_F}) \tag{4.5}$$

where $W(t)$ is the controllability grammian of the system, defined by

$$W(t) = \int_0^t e^{\mathsf{A}\tau}\mathsf{B}\mathsf{B}^T e^{\mathsf{A}^T\tau}d\tau. \tag{4.6}$$

Using the control law (equation (4.5)) the control energy can be written as,

$$J_0 = (e^{\mathsf{A}t_f}x_0 - x_{t_f})^T W(t)^{-1}(e^{\mathsf{A}t_f}x_0 - x_{t_f}). \tag{4.7}$$

This energy depends on $W^{-1}(t)$ that is, if any eigenvalue of $W(t)$ is small, then there will be at least one structural mode that is difficult to control. The minimal energy expression (4.7), depends on the matrix B and in turn depends on the actuator locations. Hence the desired locations of actuators can be found by minimizing some measure of the matrix $W^{-1}(t)$. Different scalar quantitative measures of controllability are used, such as maximizing the trace of the grammian, and maximizing the grammian eigenvalues in order to obtain the optimal locations for the actuator. The controllability grammian matrix satisfies [40]

$$\dot{W}(t) = \mathsf{A}W(t) + W(t)\mathsf{A}^T + \mathsf{B}\mathsf{B}^T.$$

When A is an asymptotically stable matrix, $W(t)$ reaches a steady state W_c as $t \to \infty$ that is the solution of the Lyapunov equation

$$\mathsf{A}W_c + W_c\mathsf{A}^T + \mathsf{B}\mathsf{B}^T = 0. \tag{4.8}$$

Controllability based placement of actuators was first used by Ami Arbel [3] to find the actuator locations in large space structures. Hac and Liu [21] extended this approach for finding sensor locations also by solving the dual problem. Sadri *et al* [54], Leleu *et al* [35] and Bruant *et al* [6],[7] have also used this method for optimal location problems.

In most of the structural dynamic cases a reduced system is considered for the analysis. This is achieved by transforming the system into modal coordinates and including only the first few modes. The displacement vector $\{q\}$ is chosen to be the modal basis of the conservative eigenmodes as,

$$\{q\} = [\phi]\{\eta\}$$

where $[\phi]$ is the modal matrix of $[M]$ and $[K]$ and $\{\eta\}$ is the modal coordinate vector. The

second-order system (equation (4.1)) can be written using modal coordinates as

$$[\tilde{M}]\{\ddot{\eta}\} + [\tilde{C}]\{\dot{\eta}\} + [\tilde{K}]\{\eta\} = \{\tilde{F}\}\{u\}$$

where,

$$[\tilde{M}] = [\phi]^T[M][\phi]$$
$$[\tilde{K}] = [\phi]^T[K][\phi]$$
$$[\tilde{C}] = [\phi]^T[C][\phi]$$
$$[\tilde{F}] = [\phi]^T[F]$$

and they can be written in state space form as,

$$\begin{aligned} \{\dot{z}\} &= [\tilde{\mathsf{A}}]\{z\} + [\tilde{\mathsf{B}}]\{u\} \\ \{x\} &= [\tilde{\mathsf{C}}]\{z\} \end{aligned} \tag{4.9}$$

where $\{z\} = \{\ q \quad \dot{q}\ \}^T$ is the transformed state vector. The matrices $[\tilde{\mathsf{A}}]$ and $[\tilde{\mathsf{B}}]$ are defined as in equation (4.3). This transformed system can now be solved for the optimal locations of actuator by minimizing the input energy (in this case modal cost function) based on a measure of modal controllability of the desired number of modes [2],[60],[54], and [22]. The most popular measure of modal controllability is the one that exploits the properties of the angle between the left eigenvector of $[\tilde{\mathsf{A}}]$ of equation (4.9) and columns of matrix $[\tilde{\mathsf{B}}]$, proposed by Hamdan and Nayfeh [22]. Assume that $[\tilde{\mathsf{A}}]$ has a set of distinct eigenvalues $\{\lambda_i\ i = 1, \cdots, n\}$ with a set of right eigenvectors and corresponding set of left eigenvectors $\{[\tilde{\mathsf{A}}]q_i = \lambda_i q_i\ i = 1, \cdots, n\}$, that are normalized so that $q_i^T p_i = \delta_{ij}$. Let L^T be an $n \times n$ matrix whose ith row is q_i^T. If ith entry in $L^T\tilde{\mathsf{B}}$ is zero, that is $q_i^T b_j = 0$ where b_j is the jth column of $\tilde{\mathsf{B}}$, then the ith mode is not controllable from all inputs [22]. This shows that the magnitude of $\left|q_i^T b_j\right|$is an indication of the controllability of the ith mode

from the jth input. It depends on the magnitudes of q_i and b_j and $\cos\theta_{ij}$ where $\theta_{ij}$is the angle between the two subspaces spanned by each of the vectors. Thus, a measure of modal controllability of the ith mode from jth actuator input of the system is cos θ_{ij}, where θ_{ij} is the angle between $b_j$and q_i as follows

$$\cos\ \theta_{ij} = \frac{\left|q_i^T b_j\right|}{\|q_i\|\ \|b_j\|}$$

The norm of the vector f_i, where $f_i^T = q_i^T[\tilde{\mathsf{B}}]/\ \|q_i\|$, is a gross measure of modal controllability of the ith mode from all inputs and this is widely used in the literature for vibrating systems [7, 22]. A variation of the above proposition was given by Choi *et al* [25] to reflect the magnitude of each element of the input matrix.

The second common type of criterion for actuator location uses a linear quadratic controller design method to find the optimal locations for actuators as well as the feedback gain [60]. The objective in the optimal control problem is to find the control $u(t)$ defined on $t \in [t_0, t_f]$ that takes the system from a given initial state $x(t_0)$ to the desired final state $x(t_f)$ in such a way that the performance function is minimized. The quadratic performance function is,

$$J = \min_u \frac{1}{2}\int_0^\infty (x^T[\mathsf{Q}]x + u^T[\mathsf{R}]u)dt \tag{4.10}$$

subject to dynamics

$$\dot{x} = \ \mathsf{A}x + \mathsf{B}u\ ;\ x(0) = x_0$$
$$0 < t < t_f.$$

The matrix [Q] is a positive semi-definite weighing matrix and the matrix [R] is a positive definite weighting matrix. It is assumed that the pair (A, B) is stabilizable. (The pair

(A, B) is stabilizable if there exists K such that $\mathsf{A} - \mathsf{BK}$ is Hurwitz [42].) The state feedback control law,

$$u(t) = -\mathsf{K}x(t)$$

solves the linear quadratic problem (4.10), where

$$\mathsf{K} = \mathsf{R}^{-1}\mathsf{B}^T\mathsf{S}$$

where S is the unique positive semi-definite solution of *the algebraic Riccati equation*,

$$\mathsf{A}^T\mathsf{S} + \mathsf{SA} - \mathsf{SBR}^{-1}\mathsf{B}^T\mathsf{S} + \mathsf{Q} = 0.$$

The optimal cost is

$$J_{opt} = \frac{1}{2}x^T(t_0)\mathsf{S}x(t_0). \tag{4.11}$$

The LQR method is used to find the optimal gain and the placement of actuators for the desired number of modes of excitation in [19, 59].

4.1.2 Optimization procedures

After choosing the objective function the problem in hand is a constrained nonlinear optimization. One of the optimization procedures used in this area is a technique proposed by Geromel [19]. Consider a discrete version of the system by a discretization of the domain, in which an optimal location needs to be found for the actuator, into N predefined points, which yields the set of input matrices $\{B_j = B(p_j)\ j = 1 \cdots N\}$. A vector $\pi = [\pi_1, \cdots, \pi_N]^T$can be assigned with the values $\pi_i = 1$ if there exists an actuator at

position p_i, and $\pi_i = 0$ otherwise. A set Φ can be defined as

$$\Phi = \{\pi \in \mathbb{R}^{\mathrm{N}} \; s.t. \; \pi \in \{0,1\}; \; \sum_{j=1}^{N} \pi_j \leq M\},$$

where M is the number of actuators. The control design problem of finding locations to optimize a linear-quadratic criterion can be written as,

$$J = \min_{\pi \in \Phi} \min_{u \in L_2} \; \frac{1}{2} \int_0^{t_f} \{y^T \mathsf{Q} y + \sum_{j=1}^{N} \pi_j u_j^T \mathsf{R}_j u_j\} dt \tag{4.12}$$

subject to

$$\dot{x} = \mathsf{A}x + \mathsf{B}u_j \quad x(0) = \xi \tag{4.13}$$

where R and B are defined as:

$$\begin{aligned} \mathsf{R} &= \textit{block diagonals}\{\pi_1 \mathsf{R}_1, \cdots, \pi_N \mathsf{R}_N\} \\ \mathsf{B} &= \sum_{j=1}^{N} \pi_j \mathsf{B}_j = [\pi_1 \mathsf{B}_1, \cdots, \pi_N \mathsf{B}_N] \end{aligned}$$

where $\mathsf{Q}, \mathsf{R}_j > 0 \; j = 1 \cdots N$, and B_j is a set of input matrices. The optimization problem can now be considered as a problem of finding $\pi \in \Phi$ such that J_{opt} will be minimized:

$$J_{opt} = \min_{\pi \in \Phi} \frac{1}{2} x^T(t_0) \mathsf{S}(t_f) x(t_0).$$

In order to minimize J with respect to $\pi \in \Phi$, it is necessary to choose a measure $\sigma(.)$ such as $\frac{1}{2} trace\{\mathsf{S}(\pi)\Xi\}$, associated with S and minimize it over Φ. The control design problem

can be written as a projection of equations (4.12) and (4.13) in to $\pi-$space as:

$$\min \{\sigma(\pi);\ \pi \in \Phi\}. \tag{4.14}$$

It may be noted from equation (4.14) that the variable π has been isolated from the control u that is the minimization problem now only depends on the location.

An important property, convexity, is proved by Geromel [19]. Define a convex set Φ_c, where $\Phi \subset \Phi_c$ as

$$\Phi_c = \{\pi \in \mathbb{R}^N \ s.t.\ \pi \geq 0\}$$

and choose a measure associated with S, $\sigma_o(\pi) : \Phi_c \mapsto \mathbb{R}$, where

$$\sigma_o(\pi) = \frac{1}{2} trace\{\mathsf{S}(\pi)\Xi\}$$

and $\Xi = \sum_{j=1}^{N} x(0)_j x^T(0)_j$. For any $\pi_0 \in \Phi_c$, define the matrices $L_j \triangleq \mathsf{B}_j \mathsf{R}_j^{-1} \mathsf{B}_j^T$, $j = 1, \cdots, N$ and

$$\mathsf{S}(\pi_0) \triangleq -\frac{1}{2} \int_0^{t_f} \mathsf{S}(\pi_0, t)\Psi(\pi_0, t)\Xi\Psi(\pi_0, t)^T \mathsf{S}(\pi_0, t)dt$$

where Ψ is the transition matrix, and then with $\mu(\pi_0) \triangleq [\mu_1(\pi_0), \cdots, \mu_N(\pi_0)]$ and $\mu_j(\pi_0) = trace\{L_j S(\pi_0)\}$, $\sigma_0(\pi) : \Phi_c \mapsto \mathbb{R}$ is convex for Ψ, $\mu(\pi_0) \in \partial\sigma_0(\pi_0)$. The convexity of the measure σ_0 ensures the global solution of equation (4.14). The global solution of the problem can be obtained using the following procedure:

Step 1: Let the initial guess of the optimal location be $\pi^0 \in \Phi$. Solution of the Riccati equation will give $\sigma(\pi^0)$.Calculate $\mu^0 = \mu(\pi_0) \in \partial\sigma(\pi^0)$, set $k = 0$ and choose $\epsilon > 0$ sufficiently small, for instance 0.001.

Master problem: It is linear 0-1 mixed program, and $\mu^i = \mu^i(\pi^i) \leqq 0$ and $d(\pi^i) = \sigma(\pi^i) -$

$\langle \mu^i, \pi^i \rangle \geqq 0$ for all $i = 0, \ldots, k$. Solution for a special case when $M = 1$ and $\phi_\infty = \Phi$ is

$$\theta^{k+1} = \min_{1 \leq j \leq N} \max_{0 \leq i \leq k} \{d(\pi^i) + \mu_j(\pi^j)\}.$$

If j^* is the optimal index, then $\pi_j^{k+1} = 1$ for $j = j^*$ and $\pi_j^{k+1} = 0$ for $j \neq j^*$.

Step 2: Solve the relaxed master problem

$$\min_{\theta, \pi \in \Phi} \{\theta : \theta \geqq \sigma(\pi^i) + \left\langle \mu^i, \pi - \pi^i \right\rangle \ i = 1 \cdots k\}.$$

Let θ^{k+1}, π^{k+1} be the optimal solution.

Step 3: Solve the Riccati equation and obtain $\sigma(\pi^{k+1})$. if $\sigma(\pi^{k+1}) - \theta^{k+1} \leqq \epsilon$, terminate. Otherwise determine μ^{k+1}, increase k by one and return to step 2.

This procedure will generate a feasible sequence π^k which converges to the global solution of joint actuator location and control problem because of the convexity. The convergence is assured in finite number of cycles that depends upon the accuracy ε. This procedure is used in finding the optimal location of a sensor, by directly minimizing a measure of observability of a reduced model of a vibrating system [52]. This procedure is well suited to use with finite elements as the integer π can be easily constructed with element-wise consideration if one whole element is considered as one piezoelectric patch.

Finding the global minimum is not guaranteed if the problem is nonconvex. The selection of a particular method is problem dependent and there is no universal algorithm for all the problems. The nonlinear constrained optimization problem can be solved using standard nonlinear programming techniques. Either direct-search or descent methods can be employed. The latter can be used for problems with a large number of variables [49] but it requires the calculation of the gradient of the performance function. The constrained

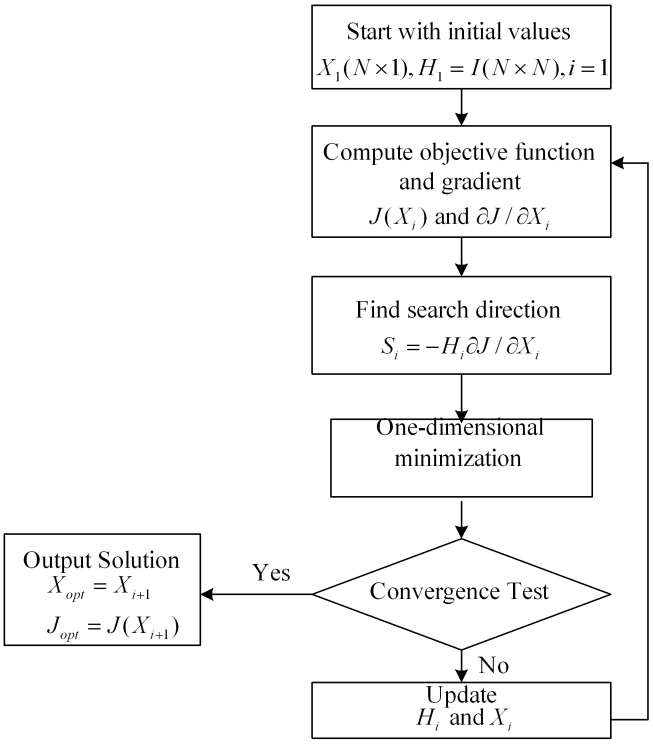

Figure 4.1: Flowchart of DFP algorithm

nonlinear problem can be mathematically written as unconstrained problem as long as the subspace of the problem is a polygon or other well-defined geometries. One robust gradient based unconstrained optimization technique, the Davidon-Fletcher-Powell algorithm [49], used in finding optimal location of actuators, sensors and optimal gain by Xu *et al* [60] is outlined in the flow chart (Figure 4.1) . Analytical expressions were derived in [60] for the gradients of the performance function with respect to actuator placement matrix B and control gain K in order to avoid the numerical difficulties encountered when finite differences were used in gradient calculations. The basic parameters for each iteration i are the vector of optimization variables X_i, an approximate inverse of the Hessian matrix H_i, and a search direction vector S_i. After finding the search direction, the one-dimensional

minimization is used find the local minimum. An accelerated step-size algorithm is used to determine an interval in the direction of search that contains at least one local minimum.

4.1.3 Numerical simulation and results

A beam made of aluminum, having a pair of linear actuators placed on either side is considered to illustrate the optimization procedures with different objective functions. The dynamic equation of the beam is solved using finite elements. This beam finite element code treats the beam and piezoelectric materials as linear elastic materials and uses linear electro-mechanical relationship for stress and strain. Each element has two nodes and has two degrees of freedom per node, and one electric degree of freedom per piezoelectric layer. Each element is considered as having no patch or being fully covered with piezoelectric material inducing equal and opposite piezoelectric moments at the nodes [13]. Shear strains are not considered in this analysis as the objective is to verify the optimization algorithm. The thickness of the bonding layer is omitted for simplicity. The optimal location obtained from the procedure is used to find the optimal shape, again using the finite element procedure. Simply supported and fixed-free boundary conditions were used in the analysis. The properties of aluminum beam are summarized in Table 4.1.

Table 4.1: Material properties of beam

Property	Aluminum	PZT
Young's Modulus GPa	79	63
Cross-Section mXm	0.05X0.01	0.05X0.0002
Length m	0.5 m	0.05 m
Density kg/m^3	2500	7600
Piezoelectric Constant d_{31} m/V	-	-254×10^{-12}

A cantilever beam is modeled with 10 beam elements as shown in Figure 4.2-a . The best

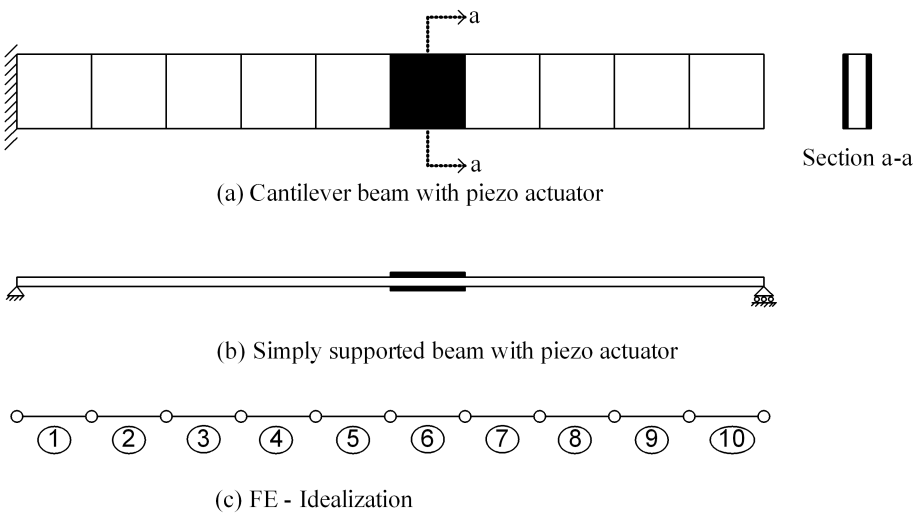

Figure 4.2: FE idealization of beam with actuator

location of one piezoelectric actuator is found using the LQR based algorithm [19] to be location 6 with seven iterations with $\mathsf{Q} = \mathsf{C}^T\mathsf{C}$ where $\mathsf{C} = [\ I \quad 0\ ]$ and $\mathsf{R} = 1$. The dynamic simulation of the beam with uniformly distributed load of $5\sin t\mathrm{N/m}$ applied through out the beam and a voltage of $100\sin t\mathrm{V}$ is applied to the actuators placed at optimal location is done for 10 sec using the Matlab lsim function. An optimal feedback controller is designed using the gain obtained from Matlab's lqr function and the controlled system is compared with uncontrolled one in Figure 4.3.Controlled response of the beam when the actuator is placed at different location, position 3, is also given in the same figure. Step response and impulse response for the system is given in Figure 4.4.

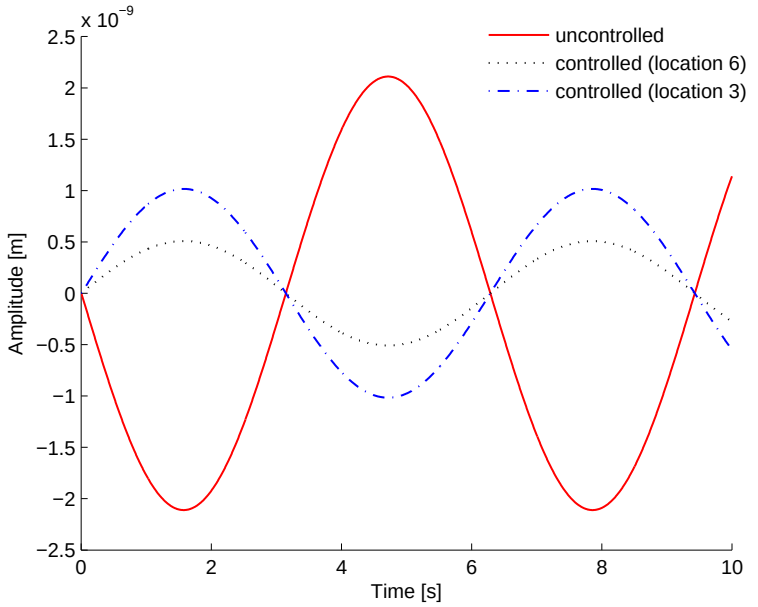

Figure 4.3: Dynamic response of cantilever beam

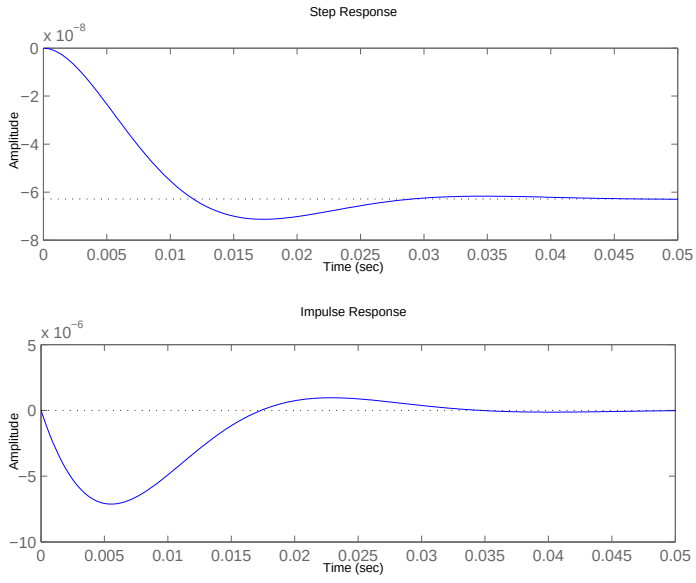

Figure 4.4: Step and Impulse response

A simply supported beam is modeled with 10 beam elements as shown in Figure 4.2-b. The best location of the piezoelectric actuator is found using the LQR based algorithm [19] to be location 3 with five iterations with $\mathsf{Q} = \mathsf{C}^T\mathsf{C}$ where $\mathsf{C} = [\ I \quad 0\ ]$ and $\mathsf{R} = 1$. Dynamic simulation of the beam with $5\sin t$ N/m distributed load and $100\sin t$V applied to the actuators placed at the optimal location is done for 10 sec, and compared with an optimal controlled model in Figure 4.5. Controlled response of the beam when the actuator is placed at different location, position 7, is also given in the same figure.

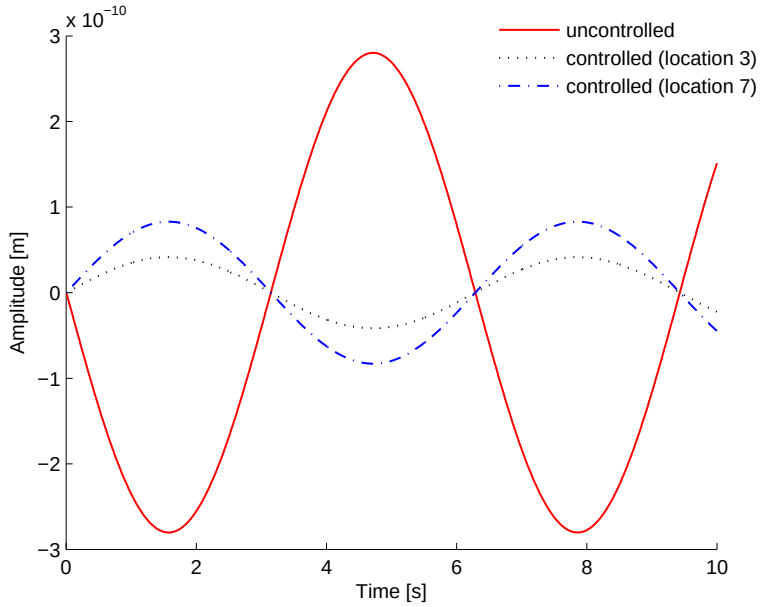

Figure 4.5: Dynamic behavior of simply supported beam

In order to verify the controllability measures, the rank test on controllability matrices was carried out for cantilever beam case. The controllability matrices had full rank for reduced systems with order up to 5 and have lower rank for the higher order systems. This shows that controllability matrices are not useful for actuator placement problems of higher order systems.

In order to find the optimal location of an actuator on a plate the following example is considered. A square (0.4×0.4m) four layer (0°/30°/0°/30°) composite plate with boundary conditions as shown in Figure 4.6 and with material properties as in Table 4.2 having a single piezoelectric patch is modelled.

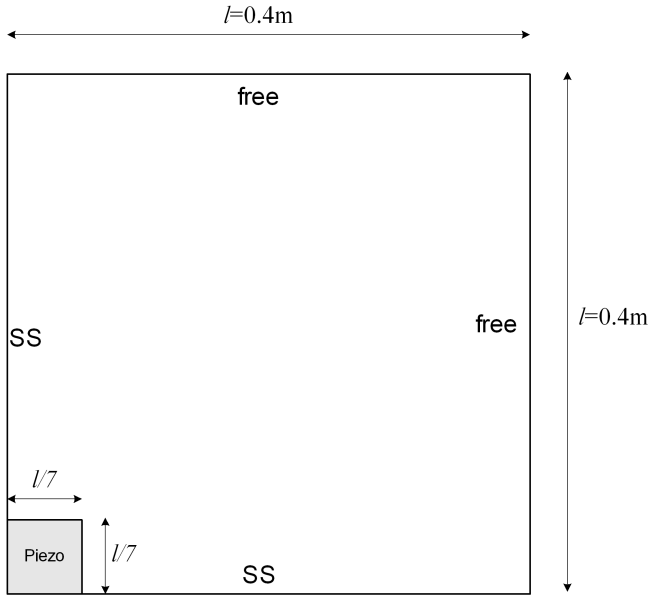

Figure 4.6: Optimal location of actuator on a plate - geometry

Table 4.2: Materials properties of plate for optimal location

	PZT G-1195	T300/976
Y_{11} GPa	63	150
Y_{12} GPa	63	9
ν	0.29	0.3
G_{12} GPa	24.8	7.1
G_{13} GPa	-	7.1
G_{23} GPa	-	2.5
Density kg/m^3	7600	1600
d_{31} pm/V	-166	-
d_{32} pm/V	-166	-

Figure 4.7 shows the FE meshing, initial location of actuator (location-1) and the optimal location (location-33) obtained from the LQR based algorithm.

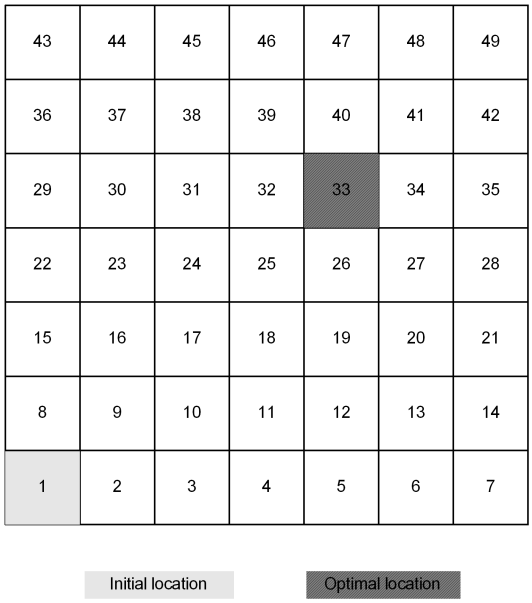

Figure 4.7: Optimal location of actuator on plate

4.2 Static shape control

The cost function used for static shape control by some authors [1, 29, 58, 62] involves the squared difference between the actual and desired shape of the structure, i.e.

$$J = \int_0^L [y(x) - y_d(x)]^2 dx$$

where $y(x)$ is the actual shape achieved by the input and $y_d(x)$ is the desired shape. Some constraints are obtained from the limits of the geometry

$$0 \leq x_i \leq L \ (i = 1, 2 \cdots n)$$

and the voltage input should lie within the limit

$$V_{min} \leq V_i \leq V_{max}.$$

In [48], analytical gradient expressions were developed using laminated composite plate theory to avoid the numerical estimation of gradient, during the optimization procedure. A gradient free optimal distribution utilizing the finite element disctretization for static shape control based on the residual voltages is presented in [43]. The objective here is to minimize the quadratic measure of the residual deviation of the current deformations of the structure from its desired state. The main advantage of this idea is to use the discretization of the domain, hence implementing it in finite element model is convenient. The steps involved in this are:

1. Discretize the structure (use FE mesh).

2. Calculate the sensor voltage V_s in each element under applied load using finite element solution.

3. Begin the shape design by assuming actuators in all the elements and then by killing the undesired actuators. The initial guess of the undesired actuators are defined by the physical boundaries of the structure. The actuators that surrounds the front are candidates for state change, a front is the set of elements which has no actuators resulting after the killing.

4. The structure is analyzed based on the current actuator configuration under unit voltage, and the required actuation voltages developed due to current actuator configuration V_a are calculated.

5. The voltages V_s and V_a are normalized with respect to their maximum values as $\bar{V}_s = \frac{V_s}{(V_s)_{max}}$, $\bar{V}_a = \frac{V_a}{(V_a)_{max}}$. Then the residual voltages V_r for the candidate elements are determined as $V_r = \bar{V}_s - \bar{V}_a$. The elements that have negative residuals are potential actuators to be removed.

6. The quadratic measure of the global residual deviation in deformation is calculated as $\alpha = \sum_{i=1}^{ndof} (\delta_i - \delta_0)$.

7. Repeat steps 4-6 until α is acceptably small.

Chapter 5

Conclusions

A summary of this thesis and conclusions arrived from the work are discussed in this chapter.

5.1 Summary and Conclusions

Optimal placement of piezoelectric actuators for the shape control of flexible structures and their modeling using finite element method is discussed in this thesis. Elastic composite plates were considered as the base structure. Modeling of composite plates with higher order plate theory were adopted from the literature [50] and finite element formulation was done and a finite element program using MATLAB was developed.

Smart structures (plate structures) with piezoelectric actuators and sensors with linear model and no hysteresis for shape control applications were modeled in Chapter 3. The plate formulation discussed earlier was modified to include the added piezoelectric layers to the plate substrate. The finite element program was modified to include piezoelectric layers in order to model smart structures. A special assembly procedure was used to

account for the piezoelectric actuator patches instead of complete layers of piezoelectric material throughout the structures. Numerical simulation of composite plate structures with linear piezoelectric actuators was done and the results were discussed. The importance of piezoelectric patches and their optimal placement were also discussed with different patch configurations and the results were given. The nonlinear electro-mechanical behavior (hysteresis) of the piezoelectric materials plays a role in shape-control applications and its inclusion in the fundamental equation was also discussed. In order to achieve a truly co-located behavior of actuators and sensors, the the self sensing actuator concept proposed by Dosch *et al* [16] was used. Implementation of self sensing actuator concept in finite element was also discussed.

A review of different methods used to construct the cost function for the optimization problem of finding the actuator/sensor locations in smart structures was discussed in Chapter 4. LQR-based methods were considered for further use. An optimization algorithm, proposed by Geromel [19] was discussed. This method is used with the finite element program developed herein to find an optimal location of one actuator on beam and plate structures and the results were given in Chapter 4. Static shape control strategies were also discussed.

5.2 Further study

Further study in this area may mainly focus on (i) experimental verification of the model (ii) extension of the optimization procedure used for the plate structures with multiple actuators, (iii) investigating possible problems in LQ control when considering non-linearities and hysteresis (iv) investigating the possibilities of other objective functions for optimal actuator location.

In the experimental part, the objective is to verify the modeling and optimization results.

Experimental setup consisting of a composite plate with self-sensing piezoelectric actuator patches located at the optimal locations found from the modeling, a precision position measuring device and a control system is required for further study. Figure 5.1 shows the schematic of such an experimental setup. A similar setup with SSA-Bridge and controller

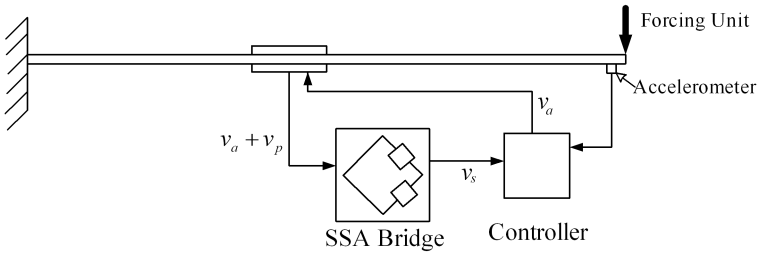

Figure 5.1: Schematic of proposed experimental setup

can be used for shape control or vibration control applications with accelerometer. The calibration of the experiment may need optical methods of displacement measurement. Implementation and testing of the hysteresis model need to be done in-order to examine the nonlinear electro-mechanical effects.

Bibliography

[1] Brij N Agarwal and Kirk E Treanor. Shape control of a beam using piezoelectric actuators. *Smart Materials and Structures*, 8:729–740, 1999.

[2] Osama J Aldraihem, Tarunraj Singh, and Robert C Wetherhold. Optimal size and location of piezoelectric actuator/sensors: Practical considerations. *Journal of Guidance, Control, and Dynamics*, 23(3):509–515, 2000.

[3] Ami Arbel. Controllability measures and actuator placement in oscillatory systems. *International Journal of Control*, 33(3):565–574, 1981.

[4] Yuanqiang Bai, Karolos M Grigoriadist, and Michael A Demetriod. H collocated control of structural systems: an analytical bound approach. In *Proceeding of the 2004 American Control Conference*, pages 2081–2086, 2004.

[5] A Benjeddou, V Gorge, and R Ohayan. Use of piezoelectric shear response in adaptive sandwich shells of revolution - part 1: Theoretical formulation. *Journal of Intelligent Material Systems and Structures*, 12:235–245, 2001.

[6] I Bruant, G Coffignal, and F Lene. A methodology for determination of piezoelectric actuator and sensor location on beam structures. *Journal of Sound and Vibration*, 243(5):861–882, 2001.

[7] I Bruant and L Proslier. Optimal location of actuators and sensors in active vibration control. *Journal of Intelligent Material System and Structures*, 16:197–206, 2005.

[8] W G Caddy. *Introduction to the theory and application of electromechanical phenomena in crystals, VOL I &II.* Dover Publications inc, 1964.

[9] Young Hwan Chang, Do Hyung Kim, In Lee, and Jae Hung Han. A patch-type smart self-sensing actuator. *Smart Materials and Structures*, 15:667–677, 2006.

[10] Chen Chang-Quing, Wang Xiao-Ming, and Shen Ya-Peng. Finite element approach of vibration control using self-sensing piezoelectric actuators. *Computers and Structures*, 60(3):505–512, 1996.

[11] P Chen and S Montgomery. A macroscopic theory for the existence of the hysteresis and butterfly loops in ferroelectricity. *Ferroelectrics*, 23:199–207, 1980.

[12] Q H Cheng, T S Lok, and Z C Xie. Geometrically non-linear analysis including shear deformation of composite laminates. *Thin-Walled Structures*, 35(1):41–59, 1999.

[13] E F Crawley and J Louis. Use of piezoelectric actuators as elements of intelligent structures. *AIAA Journal*, 25:1373–1385, 1987.

[14] D T Detwiler. Finite element analysis of laminated composite structures containing distributed piezoelectric sensors and actuators. *Finite Elements in Analysis and Design*, 20:87–100, 1995.

[15] T Doong and I Mayergoyz. On numerical implementation of hysteresis models. *IEEE Transactions on Magnetics*, 21:1853–1855, 1985.

[16] Jeffrey J Dosch, Daniel J Inman, and Ephrahim Garcia. A self sensing piezoelectric actuator for collocated collocated control. *Journal of Intelligent Materials Systems and Structures*, 3:166–185, 1992.

[17] Luc R Dupre, Roger Van Keer, and Jan A A Melkebeek. Identification of the relation between the material parameters in the presach model and in the jiles-atherton hysteresis model. *Journal of Applied Physics*, 85:4376–4378, 1999.

[18] Ping Ge and Musa Jouaneh. Modelling hysteresis in piezoceramic actuators. *Precision Engineering*, 17(3):211–221, 1995.

[19] Jose C Geromel. Convex analysis and global optimization of joint actuator location and control problems. *IEEE Transactions on Automatic Control*, 34(7):711–719, 1989.

[20] S K Ha. Finite element analysis of composite structures containing distributed piezoelectric sensors and actuators. *AIAA Journal*, 30:772–780, 1992.

[21] A Hac and L Liu. Sensor and actuator location in motion control of flexible structures. *Journal of Sound and Vibration*, 167:239–261, 1993.

[22] A M A Hamdan and A H Nayfeh. Measures of modal controlability and observability for first and second order linear systems. *Journal of Guidance*, 12(3):421–428, 1989.

[23] Declan Hughes and John T Wen. Preisach modeling of piezoceramic and shape memory alloy hysteresis. *Smart Materials and Strictures*, 6:287–300, 1997.

[24] W S Hwang and H C Park. Finite element modelling of piezoelectric sensors and actuators. *AIAA Journal*, 31(5):930–937, 1993.

[25] Y. Kim J. W. Choi, J. G. Lee and T. Kang. Design of an effective controller via accommodating left eigenstructure assignment. *Journal of Guidance,Control, and Dynamics*, 18(2):347–354, 1995.

[26] Lowell Jones, Ephrahim Garcia, and Henry Waitest. Self-sensing control as applied to a pzt stack actuator used as a micropositioner. *Smart Materials and Structures*, 3:147–156, 1994.

[27] T L Jorden and Z Ounaies. Piezoelectric ceramics characterization. report 2001-28, ICASE, 2001.

[28] Bryson A E Jr and Ho Y C. *Applied Optimal Control: Optimization, Estimation, and Control*. Hemisphere, 1975.

[29] J C Bruch Jr, J M Sloss, S Adali, and I S Sadek. Optimal piezo-actuator locations-lengths and applied voltage for shape control of beams. *Smart Materials and Structures*, 9:205211, 2000.

[30] R E Kalman, Y C Ho, and K S Narendra. Controllability of linear dynamical systems. *Contributions to Differential Equations*, 1(2):189–213, 1963.

[31] Marc Kamlah, Ulrich Bohle, and Dietrich Munz. On a nonlinear finite element method for piezoelectric strucutres made of hysteretic ferroelectric ceramics. *Computational Materials Science*, 19:81–86, 2000.

[32] K Y Lam. A finite-element based model for piezoelectric composite laminates. *Smart Materials and Structures*, 6:583–591, 1997.

[33] W W Law, W H Liao, and J Huang. Vibration control of structures with self-sensing piezoelectric actuators incorporating adaptive mechanisms. *Smart Materials and Structures*, 12:720–730, 2003.

[34] T Leigh and D Zimmerman. An implicit method for the nonlinear modelling of piezoelectric actuators displaying hysterisis. *Smart Structures and Materials*, 123:57–63, 1991.

[35] Sylvaine Leleu, Hisham Abou-Kandil, and Yvan Bonnassieux. Piezoelectric actuators and sensors location for active control of flexible structures. *IEEE Transaction on Instrumentation and Measurement*, 50(6):1577–1582, 2001.

[36] W H Liao, W W Law, and K W Chan. Implementation of adaptive structures with enhanced self-sensing piezoelectric actuators. In *IEEE International Conference on Industrial Technology 2002*, 2002.

[37] K M Liew, H K Lim, M J Tan, and X Q He. Analysis of laminated composite beams and plates with piezoelectric patches using the element-free galerkin method. *Computational Mechanics*, 29:486–497, 2002.

[38] G R Liu, X Q Peng, and K Y Lam. Vibration control simulation of laminated composite plates with integrated piezoelectrics. *Journal of Sound and Vibration*, 220(5):827–846, 1999.

[39] W P Mason. Piezoelectricity, its history and application. *Journal of Acoustic Society of America*, 70(6):1561–1566, 1981.

[40] Richard H Middleton and Graham C Goodwin. *Digital control and estimation: a unified approach*. Prentice Hall, 1990.

[41] Jose M Simoes Moita, Cristovao, M Mota Soares, and Carlos A Mota Soares. Geometrically nonlinear analysis of composite strucutes with integrated piezoelectric sensors and actuators. *Composite Structures*, 57:253–261, 2002.

[42] Kirsten Morris. *Introduction to Feedback Control*. Harcourt/Academic Press, 2001.

[43] A Mukherjee and S P Joshi. A gradientless technique for optimal distribution of piezoelectric material for structural control. *International Journal for Numerical Methods in Engineering*, 57:1737–1753, 2003.

[44] Chao C P Paul, C W Chiu, J S Huang, and H C Tseng. Dynamic finite element analysis of a piezoelectric bimorph beam deflector with consideration of hysteresis effect. In *Proceedings of DETC'03*, pages 1851–1856, 2003.

[45] Ramesh Periasamy. Nonlinear analysis of piezolaminated plates. Master's thesis, Indian Institue of Technology, Madras, India, 2004.

[46] A Pica, R D Wood, and E Hinton. Finite element analysis of geometrically nonlinear plate behavior using midlin formulation. *Composites and Structures*, 11:203–215, 1980.

[47] Farzad Pouboghart, Harin Pongpairoj, Il-Jin Youn, Ramesh Balasubramanian, Raguram Radhakrishnan, Morteza Daneshoost, and Mohamed Sayeh. Vibration control of flexible structures using self sensing actuators. *SPIE*, 3668:950–959, 1999.

[48] Sedaghati R and A Zabihollahand Mi Ahar. Sensitivity analysis and optimal design of smart piezolaminated composite beams. *AIAA Journal*, 44(12):2987–2996, 2006.

[49] Singiresu S. Rao. *Engineering Optimization*. John Wiley & Sons, Inc, 1996.

[50] J N Reddy. *Mechanics of laminated composite plate, Theory and analysis*. CRC Press, 1996.

[51] J N Reddy and W C Chao. Nonlinear bending of thick rectangular, laminated composite plate. *International Journal of Nonlinear Mechanics*, 16(3/4):291–301, 1981.

[52] Marie Reynier and Hisham Abou-Kandil. Sensor location for updating problems. *Mechanical Systems and Signal Processing*, 13(2):297–314, 1999.

[53] Zaghloul SA and Kennedy JB. Nonlinear behaviour of symmetrically laminated plates. *Journal of Applied Mechanics*, 42:234–236, 1975.

[54] A M Sadri, J R Wright, and R J Wynne. Modelling and optimal placement of piezoelectric actuators in isotropic plates using genetic algorithms. *Smart Materials and Structures*, 8:490–498, 1999.

[55] G Sing and Y V K Sadasiva Rao. Large deflection behavior of thick composite plates. *Composite strucutres*, 8:13–29, 1987.

[56] Ralph C Smith. *Smart material systems.* SIAM, 2005.

[57] H S Tzou and C I Tseng. Distributed piezoelectric sensor/actuator design for dynamic measurement/control of distributed parameter systems: A piezoelectric finite element approach. *Journal of Sound and Vibration*, 138(1):17–34, 1990.

[58] Varadharajan. Adaptive shape control of laminated composite plates. *AIAA Journal*, 3:1694–1698, 1998.

[59] Gordon Parker Wei Chen, Markus Buehler and Bernhard Bettig. Optimal sensor design and control of piezoelectric laminate beams. *IEEE Transactions on Control Systems Technology*, 12(1):148–155, 2004.

[60] K Xu, P Warnitchai, and T Igusa. Optimal placement and gains of sensors and actuators for feedback control. *Journal of Guidance, Control, and Dynamics*, 17(5):929–934, 1994.

[61] Sung Y and Kam Yim Szeb. A finite element formulation for composite laminates with smart constrained layer damping. *Advances in Engineering Software*, 31:529–537, 2000.

[62] Shenguan Yang and Brain Ngoi. Shape control of beams by piezoelectric actuators. *AIAA Journal*, 38(12):2292–2298, 2000.

[63] Jessica M Yellin and I Y Shen. A self-sensing active constrained layer damping treatment for a euler-bernoulli beam. *Smart Materials and Structures*, 5:628–637, 1996.

Appendix A

Transformations

Coordinate, stresses, strains and material coefficients are transformed form material coordinates (x_1, x_2, x_3) to problem coordinates (x, y, z) using transformation matrices based on particular transformation, rotation about a transverse normal to the lamina, refer to Figure 2.4. The transformed elastic coefficients given in equation (2.5) have the form,

$$\overline{Q} = \begin{bmatrix} \overline{Q}_{11} & \overline{Q}_{12} & \overline{Q}_{16} & 0 & 0 \\ \overline{Q}_{12} & \overline{Q}_{22} & \overline{Q}_{26} & 0 & 0 \\ \overline{Q}_{16} & \overline{Q}_{26} & \overline{Q}_{66} & 0 & 0 \\ 0 & 0 & 0 & \overline{Q}_{44} & \overline{Q}_{45} \\ 0 & 0 & 0 & \overline{Q}_{45} & \overline{Q}_{55} \end{bmatrix}$$

where

$$\begin{aligned} \overline{Q}_{11} &= Q_{11}\cos^4\alpha + 2(Q_{12} + 2Q_{66})\sin^2\alpha\cos^2\alpha \\ \overline{Q}_{12} &= (Q_{11} + Q_{22} - 4Q_{66})\sin^2\alpha\cos^2\alpha + Q_{12}(\sin^4\alpha + \cos^4\alpha) \end{aligned}$$

$$
\begin{aligned}
\overline{Q}_{22} &= Q_{11}\sin^4\alpha + 2(Q_{12}+2Q_{66})\sin^2\alpha\cos^2\alpha + Q_{22}\cos^4\alpha \\
\overline{Q}_{16} &= (Q_{11}-Q_{12}-2Q_{66})\sin\alpha\cos^3\alpha + (Q_{12}-Q_{22}+2Q_{66})\sin^3\alpha\cos\alpha \\
\overline{Q}_{26} &= (Q_{11}-Q_{12}-2Q_{66})\sin^3\alpha\cos\alpha + (Q_{12}-Q_{22}+2Q_{66})\sin\alpha\cos^3\alpha \\
\overline{Q}_{66} &= (Q_{11}+Q_{12}-2Q_{12}-2Q_{66})\sin^2\alpha\cos^2\alpha + Q_{66}(\sin^4\alpha+\cos^4\alpha) \\
\overline{Q}_{44} &= Q_{44}\cos^2\alpha + Q_{55}\sin^2\alpha \\
\overline{Q}_{45} &= (Q_{55}-Q_{44})\sin\alpha\cos\alpha \\
\overline{Q}_{55} &= Q_{44}\sin^2\alpha + Q_{55}\cos^2\alpha
\end{aligned}
$$

with

$$
\begin{aligned}
Q_{11} &= Y_{11}/(1-\nu_{12}\nu_{21}) \\
Q_{12} &= \nu_{12}Y_{12}/(1-\nu_{12}\nu_{21}) \\
Q_{22} &= Y_2/(1-\nu_{12}\nu_{21}) \\
Q_{66} &= G_{12} \\
Q_{44} &= G_{23} \\
Q_{55} &= G_{13}
\end{aligned}
$$

where $Y_{11}$and $Y_{22}$are Young's Moduli and G_{12}, G_{13} and G_{23} are shear moduli in materials axis.

The piezoelectric stress coefficient matrix $[\overline{e}]$given in equation (3.1) have the form,

$$
[\overline{e}] = \begin{bmatrix} 0 & 0 & 0 & \overline{e}_{14} & \overline{e}_{15} \\ 0 & 0 & 0 & \overline{e}_{24} & \overline{e}_{25} \\ \overline{e}_{31} & \overline{e}_{32} & \overline{e}_{36} & 0 & 0 \end{bmatrix}
$$

where

$$\begin{aligned}
\overline{e}_{31} &= e_{31}\cos^2\alpha + e_{32}\sin^2\alpha \\
\overline{e}_{32} &= e_{31}\sin^2\alpha + e_{32}\cos^2\alpha \\
\overline{e}_{36} &= (e_{31} - e_{32})\sin\alpha\cos\alpha \\
\overline{e}_{14} &= (e_{15} - e_{24})\sin\alpha\cos\alpha \\
\overline{e}_{24} &= e_{24}\cos^2\alpha + e_{15}\sin^2\alpha \\
\overline{e}_{15} &= e_{15}\cos^2\alpha + e_{24}\sin^2\alpha \\
\overline{e}_{25} &= (e_{15} - e_{24})\sin\alpha\cos\alpha
\end{aligned}$$

where $[e_{ij}]$ are piezoelectric stress coefficients.

Appendix B

Strain Displacement Relation and Element matrices

Total elastic strain is given in equation (2.3). Using the shape function definition given in equation (2.16), the linear strain displacement matrix $[\mathcal{B}^{\mathrm{l}}]$ for elements can be derived and the elemental strain can be written in terms of nodal displacements $\{a^e\}$ as

$$\{\epsilon^e\} = [\mathcal{B}]\{a^e\}$$

Strain displacement matrix for linear in-plane strain components $\epsilon_p$is

$$[\mathcal{B}_P^l] = \begin{bmatrix} \partial H_i/\partial x & 0 & 0 & 0 & 0 \\ 0 & \partial H_i/\partial y & 0 & 0 & 0 \\ \partial H_i/\partial y & \partial H_i/\partial x & 0 & 0 & 0 \\ 0 & 0 & 0 & 0 & 0 \\ 0 & 0 & 0 & 0 & 0 \end{bmatrix}_{i=1\ldots4}$$

and for linear bending strain components ϵ_b is

$$[\mathcal{B}_b^l] = \begin{bmatrix} 0 & 0 & 0 & \partial H_i/\partial x & 0 \\ 0 & 0 & 0 & 0 & \partial H_i/\partial y \\ 0 & 0 & 0 & \partial H_i/\partial y & \partial H/\partial x \\ 0 & 0 & 0 & 0 & 0 \\ 0 & 0 & 0 & 0 & 0 \end{bmatrix}_{i=1\ldots4}$$

and for linear shear strain compo nets ϵ_s

$$[\mathcal{B}_s^l] = \begin{bmatrix} 0 & 0 & 0 & 0 & 0 \\ 0 & 0 & 0 & 0 & 0 \\ 0 & 0 & 0 & 0 & 0 \\ 0 & 0 & \partial H_i/\partial y & 0 & H_i \\ 0 & 0 & \partial H_i/\partial x & H_i & 0 \end{bmatrix}_{i=1\ldots4}$$

where i is node number. Nonlinear strain displacement matrix can be derived from the strain definition (equation (2.3)). The nonlinear strain components can be written as,

$$\epsilon_p^{nl} = \begin{Bmatrix} \frac{1}{2}\left(\frac{\partial w_0}{\partial x}\right)^2 \\ \frac{1}{2}\left(\frac{\partial w_0}{\partial y}\right)^2 \\ \left(\frac{\partial w_0}{\partial x}\frac{\partial w_0}{\partial y}\right) \end{Bmatrix} = \frac{1}{2}\begin{bmatrix} \frac{\partial w_0}{\partial x} & 0 \\ 0 & \frac{\partial w_0}{\partial y} \\ \frac{\partial w_0}{\partial y} & \frac{\partial w_0}{\partial x} \end{bmatrix} \begin{Bmatrix} \frac{\partial w_0}{\partial x} \\ \frac{\partial w_0}{\partial y} \end{Bmatrix} = \frac{1}{2}[\mathcal{A}][\phi]$$

where $\{\phi\}^T = \left\{ \begin{array}{cc} \frac{\partial w_0}{\partial x} & \frac{\partial w_0}{\partial y} \end{array} \right\}$ is displacement gradient with respect to lateral displacement w_0 They can be written in terms of nodal displacements using shape functions as,

$$\{\phi\} = \begin{bmatrix} 0 & 0 & \partial H_i/\partial x & 0 & 0 \\ 0 & 0 & \partial H/\partial y & 0 & 0 \end{bmatrix} \{a^e\} = [\mathcal{G}]\{a^e\}.$$

In order to derive the strain displacement relation, if we take the derivative of non-liner strain ϵ_p^{nl},

$$d\left\{\epsilon_p^{nl}\right\} = \frac{1}{2}d[\mathcal{A}]\{\phi\} + \frac{1}{2}[\mathcal{A}]d\{\phi\} = [\mathcal{A}]d\{\phi\} = [\mathcal{A}][\mathcal{G}]d\{a^e\}$$

therefore, $[\mathcal{B}^{nl}] = [\mathcal{A}][\mathcal{G}]$.

The Electric field E can be written in terms of electric potential as

$$\{E\} = [\ 0 \quad 0 \quad 1/t_k \quad 0 \quad 0\ ]^T V = [\mathcal{B}^{\phi}]V$$

because it is assumed that the electric potential is constant over an element and varies linearly through the thickness. Using the the total strain definition 3.4 and the strain displacement matrices, the linear stiffness matrices of the system (equation (3.9)) can be written as:

$$\begin{aligned} K_{uu} &= \Sigma_{k=1}^{n} \int_A \int_z [\mathcal{B}^l]^T [\overline{Q}][\mathcal{B}^l] dz dA, \\ K_{u\phi} &= \Sigma_{k=1}^{n} \int_A \int_z [\mathcal{B}^l]^T [\overline{Q}][\mathcal{B}^{\phi}] dz dA, \\ K_{\phi u} &= \Sigma_{k=1}^{n} \int_A \int_z [\mathcal{B}^{\phi}]^T [\overline{Q}][\mathcal{B}^l] dz dA, \\ K_{\phi\phi} &= \Sigma_{k=1}^{n} \int_A \int_z [\mathcal{B}^{\phi}]^T [\overline{Q}][\mathcal{B}^{\phi}] dz dA, \end{aligned}$$

the first integration is over the area of an element.

Appendix C

Matlab Code

This appendix is the Matlab source code developed in this work. The file name is code.pdf. Read the instruction in the code.pdf on how to run the program in Matlab.